

Data Set Catalog # 222

Apollo 14, 15 and 16

BISTATIC RADAR EXPERIMENT

71-008A-04A, 04B, 04C

71-063A-14A, 14B, 14C

72-031A-12A, 12B, 12C

9 tapes

---

## Table of Contents

1. Introduction
2. Errata/Change Log
3. LINKS TO RELEVANT INFORMATION IN THE ONLINE NSSDC INFORMATION SYSTEM
4. Catalog Materials
  - a. Associated Documents
  - b. Core Catalog Materials

---

## **1. INTRODUCTION:**

The documentation for this data set was originally on paper, kept in NSSDC's Data Set Catalogs (DSCs). The paper documentation in the Data Set Catalogs have been made into digital images, and then collected into a single PDF file for each Data Set Catalog. The inventory information in these DSCs is current as of July 1, 2004. This inventory information is now no longer maintained in the DSCs, but is now managed in the inventory part of the NSSDC information system. The information existing in the DSCs is now not needed for locating the data files, but we did not remove that inventory information.

The offline tape datasets have now been migrated from the original magnetic tape to Archival Information Packages (AIP's).

A prior restoration may have been done on data sets, if a requestor of this data set has questions; they should send an inquiry to the request office to see if additional information exists.

## 2. ERRATA/CHANGE LOG:

NOTE: Changes are made in a text box, and will show up that way when displayed on screen with a PDF reader.

*When printing, special settings may be required to make the text box appear on the printed output.*

Version	Date	Person	Page	Description of Change
01				
02				

3 LINKS TO RELEVANT INFORMATION IN THE ONLINE NSSDC INFORMATION SYSTEM:

<http://nssdc.gsfc.nasa.gov/nmc/>

[NOTE: This link will take you to the main page of the NSSDC Master Catalog. There you will be able to perform searches to find additional information]

4. CATALOG MATERIALS:

- a. Associated Documents      To find associated documents you will need to know the document ID number and then click here.  
<http://nssdcftp.gsfc.nasa.gov/miscellaneous/documents/>

- b. Core Catalog Materials

APOLLO 14 CSM

PSPG 00595

13 CM BISTATIC RADAR LUNAR OBS.

71-008A-04A

This data set has been restored. There was originally one 9-track, 1600 BPI tape written in Binary. There is one restored tape. The DR tape is a 3480 cartridge and the DS tape is 9-track, 6250 BPI. The original tape was created on a 930 computer and the restored tape was created on an IBM 9021 computer. The DR and DS numbers along with the corresponding D number are as follows:

DR#	DS#	D#	FILES	TIME SPAN
-----	-----	-----	-----	-----
DR005628	DS005628	D011596	1	02/06/71 - 02/06/71

APOLLO 14

PSPG - 00360

116-CM BISTATIC RADAR LUNAR OBS.

71-008A-04B

THIS DATA SET HAS BEEN RESTORED. IT ORIGINALLY CONTAINED ONE 9-TRACK, 800 BPI TAPE WRITTEN IN BINARY. THERE IS ONE RESTORED TAPE. THE DR TAPE IS A 3480 CARTRIDGE AND THE DS TAPE IS 9-TRACK, 6250 BPI. THE ORIGINAL TAPE WAS CREATED ON AN IBM 360 COMPUTER AND WAS RESTORED ON THE MRS. THE DR AND DS NUMBER ALONG WITH THE CORRESPONDING D NUMBER AND TIME SPAN IS AS FOLLOWS:

DR#	DS#	D#	FILES	TIME SPAN
DR003596	DS003596	D011595	1	02/06/71 - 02/06/71 (a)

(a) TWO READ ERRORS ON RECORDS 10 AND 7214

APOLLO 15 CSM

*PSPG 00096*

13 CM BISTATIC RADAR LUNAR OBS.

71-063A-14A

This data set has been restored. There were originally two 7-track, 800 BPI tapes written in Binary. There is one restored tape. The DR tape is a 3480 cartridge and the DS tape is 9-track, 6250 BPI. The original tapes were created on a 930 computer and the restored tapes were created on an IBM 9021 computer. The DR and DS numbers along with the corresponding D numbers are as follows:

DR#	DS#	D#	FILES	TIME SPAN
-----	-----	-----	-----	-----
DR005637	DS005637	D011591	1	08/01/71 - 08/01/71 (a)
		D011592	2	08/01/71 - 08/01/71

(a) D011591: Read error occurred in record 3147 of file 1.

APOLLO 15 CSM

PSPG 00584

116-CM BISTATIC RADAR LUNAR OBS.

71-063A-14B

This data set has been restored. There was originally one 7-track, 800 BPI tape written in Binary. There is one restored tape. The DR tape is a 3480 cartridge and the DS tape is 9-track, 6250 BPI. The original tape was created on an IBM 930 computer and the restored tape was created on an IBM 9021 computer. The DR and DS numbers along with the corresponding D number are as follows:

DR#	DS#	D#	FILES	TIME SPAN
-----	-----	-----	-----	-----
DR005894	DS005894	D011593	1	08/01/71 - 08/01/71

APOLLO 16 CSM

PSPG 00568

13-CM BISTATIC RADAR LUNAR OBS.

72-031A-12A

This data set has been restored. There were originally two 7-track, 800 BPI tapes written in Binary. There is one restored tape. The DR tape is a 3480 cartridge and the DS tape is 9-track, 6250 BPI. The original tapes were created on a XDS computer and the restored tapes were created on an IBM 9021 computer. The DR and DS numbers along with the corresponding D numbers are as follows:

DR#	DS#	D#	FILES	TIME SPAN
-----	-----	-----	-----	-----
DR005649	DS005649	D011589	1	04/23/72 - 04/23/72 (a)
		D011588	2	04/23/72 - 04/23/72

(a) D011589: Read error occurred in record 309 of file 1.

71-008A-04A

Apollo 14, 13 CM Bistatic Radar Lunar Obs.

The data is contained on one 800 BPI, 9 track, binary XDS-sigma V tape with one file. A 7 track C copy was made.

D-11596            C-09246            2/06/71 - 2/06/71

71-008A-04B

Apollo 14, 116 CM Bistatic Radar Lunar Obs.

The data is contained on one 800 BPI, 9 track, Binary, XDS-sigma V tape with one file. A 7 track C copy was made.

D-11595            C-09247            2/06/71 - 2/06/71

71-063A-14A

Apollo 15, 13 CM Bistatic Radar Lunar Obs.

The data is contained on two 800 BPI, 9 track, Binary, XDS-sigma V tapes with one file each. Two 7 track C copy's were made.

D-11591            C-09248    1 of 2    8/01/71 - 8/01/71

D-11592            C-09249    2 of 2    8/01/71 - 8/01/71

71-063A-14B

Apollo 15, 116 CM Bistatic Radar Lunar Obs.

The data is contained on one 800 BPI, 9 track, Binary, XDS-sigma V tape with one file. A 7 track C copy was made.

D-11593            C-09250            8/01/71 - 8/01/71

72-031A-12A

Apollo 16, 13 CM Bistatic Radar Lunar Obs.

The data is contained on two 800 BPI, 9 track, Binary, XDS-sigma V tapes with one file each. Two 9 track C copy's were made.

D-11589            C-09251    1 of 2    4/23/72 - 4/23/72

D-11588            C-09252    2 of 2    4/23/72 - 4/23/72

72-031A-12B

Apollo 16, 116 CM Bistatic Radar Obs.

The data is contained on one 800 BPI, 9 track, Binary, XDS-sigma V tape with one file each. A 7 track C copy was made.

D-11590

C-09253

4/23/72 - 4/23/72

71-008A-04C

71-063A-14C

72-031A-12C

Apollo 14, 15, 16 Combined Bistatic Radar Obs. <sup>D-12324</sup> C-09582

This data is contained on one 800 BPI, 9 track, Binary, XDS-sigma V tape with 6 files. A 7 track C copy was made.

<u>D#</u>	<u>C#</u>	<u>FILE</u>	<u>CONTENTS</u>	<u>DATE DATA WAS TAKEN</u>
D-1	12324	C-09582	5821 Apollo 14, 116CM	2/06/71
D-		C-	2 Apollo 14, 13 CM	2/06/71
D-		C-	3 Apollo 15, 116CM	8/01/71
D-		C-	4 Apollo 15, 13 CM	8/01/71
D-		C-	5 Apollo 16, 116CM	4/23/72
D-		C-	6 Apollo 16, 13 CM	4/23/72

July 24, 1973

To: Data Repository

From: ADP Services

Subject: Apollo 14, 15, 16 Combined Bistatic Radar tape.

Please release tape DD11594 and the corresponding DC number and return to G. R. Dow as per attached letter. A replacement tape DD12324 has been received, processed and placed in the NSSDC library.

July 24, 1973

Mr. G. R. Dow  
Center for Radar Astronomy  
Dept. of Electrical Engineering  
Stanford University  
Stanford, California 94305

Subject: Your letter and shipment of June 25, 1973, concerning  
the Bistatic Radar data tape.

Dear Mr. Dow,

We are returning, under separate cover, the magnetic tape  
containing Apollo 14, 15 and 16 Bistatic Radar data which  
you sent to us earlier this year. The replacement tape has  
been duplicated and placed in the NSSDC library. If you  
have any questions please call us.

Yours truly,

Joseph R. Johns  
Manager, ADP Services

Under Separate Cover:  
Magnetic tape containing  
Apollo 14, 15 and 16 data (1)

May 11, 1973

To: C. Wende  
From: ADP Services  
Subject: Apollo 16 Bistatic Radar data tapes

There is a data word discrepancy in the header record of the Apollo 16, Bistatic Radar data tapes. Words 43 and 44 indicate day and year that the data were collected in integer format. Word 45 and 46 also indicate Julian Ephemeris day at 00.00.00 GMT or day the data was collected in double precision format. Based on our conversion of words 43 and 44 the time the data were collected is 4/23/72. When data for words 45 and 46 were calculated on the ephemeris day program (Julian) we came up with a time that data were collected as 4/22/72. The tapes were processed using the first date; 4/23/72. If there are any objections please contact ADP Services.

APOLLO 14, 15, 16

13 cm BISTATIC LUNAR TRACKING OBS.

116 cm BISTATIC LUNAR TRACKING OBS.

Appendix IV

JM Doptrack Tape Formats

This appendix describes the tape formats for the JM Doptrack Tapes generated in Subtask 6 of the text. Tapes are 9 track, <sup>800 BPI</sup> binary in XDS Sigma <sup>Y</sup> machine images. These tapes contain the output of the polarimeter in Subtask 4, the corrected fractional polarization obtained from Subtask 5, MSC trajectory data, and certain ancillary quantities computed at Stanford. All records within the given file are the same length. There may be more than one tape per file. Files are identified by a header record which contains a brief description of the tape contents. This Appendix describes the tape organization, the file organization, and the record formats for the JM Doptrack tapes. Definitions of the tape contents are either given here or described by reference.

A. Tape Organization

File	No. Tapes	Contents	Record Length
1	1	Apollo-14 116 cm	514
2	1	Apollo-14 13 cm	514
3	1	Apollo-15 116 cm	1026
4	2	Apollo-15 13 cm	514
5	1	Apollo-16 116 cm	1026
6	2	Apollo-16 13 cm	514

B. File Organization

1. Header Record
  2. Data Record #1
  3. Data Record #2
  4. Data Record #3
  5. Data Record #4
  6. Data Record #5
  7. Data Record #6
  8.  $\vdots$
  9. ~~EOF~~ <sup>d</sup> (End of File Work)
- } Observational Data } Data Frame
- } ephemeris data }

Files may be continued across the end of a tape.

Appendix IV (cont.)

C. Header Record Formats

<u>Word No.</u>	<u>Contents</u>	<u>Units</u>	<u>Machine Type<sup>α</sup></u>
1	Alphanumeric Tape Identifier	--	A
⋮			
42			
43	Day of year on which data were collected (January 1 = day 1)		I
44	Year data were taken		I
45 }	Julian Ephemeris Day at 00:00:00 GMT on the day the data were taken	(days)	DPR
46 }			
47 }	Julian Ephemeris Day of reference epoch	(days)	DPR
48 }			
49	Time increment between data frames	(sec)	R
50	Number of data records following the Header Records (Number of data frames = Number of Data Records ÷ by 6)	--	I
50	No meaningful data		
⋮			
end			

Appendix IV (cont.)

- $\alpha$  A - Alpha numeric
- I - Integer
- R - Real
- DPR - Double precision real

D. Data Frame Formats

1. Data Record Organization

<u>Record No.</u>	<u>Contents</u>	<u>Note:</u>
1	$J_{11}(k)$	116 cm data
2	$J_{22}(k)$	$J_{11}(k)$ - <u>Left</u> circular polarization
3	Real part of $J_{12}(k)$	
4	Imaginary part of $J_{12}(k)$	$J_{22}(k)$ - <u>Right</u> circular polarization
5	$\gamma(k)$	
6	Spacecraft ephemeris and ancillary data	13 cm data
		$J_{11}(k)$ - <u>Right</u> circular polarization
		$J_{22}(k)$ - <u>Left</u> circular polarization

2. Format Records 1-5 (all machine type REAL) ✓

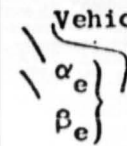
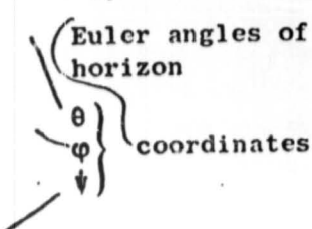
<u>Word No.</u>	<u>Contents</u>
1	Data described under D.1 above
⋮	
513/1025	
514/1026	Sequential Record No.

3. Format Record 6 (all machine type Real)

<u>Word No.</u>	<u>Contents</u>	<u>Units</u>
1	Frame No. (data record no. mod 6)	
2	UT2	(sec)
3	Difference of reflected and direct dopplers, > 0 for reflected doppler > directed doppler	(Hz)
4	Predicted bandwidth for 0.1 radian rms surface slope	(Hz)

Appendix IV (cont.)

3. Format Record 6 (all machine type Real) (cont.)

<u>Word No.</u>	<u>Contents</u>	<u>Units</u>	
5	Angle of incidence	(deg)	
6	Spacecraft altitude (mean lunar radius assumed 1736 km)	(km)	
7	Spacecraft speed	(m/sec)	
8	Radar cross section predicted for smooth conducting moon	(dim)	
9	(Radar cross section) / (received power)	(m <sup>2</sup> /w)	
10	X } Components of Selenographic unit position vector of spacecraft location	(dim)	
11			Y }
12			Z }
13	X } Components of Selenographic unit position vector of specular point location	(dim)	
14			Y }
15			Z }
16	Latitude of sub-spacecraft position	(deg)	
17	Longitude of sub-spacecraft position	(deg)	
18	Component of doppler shift due to earth rotation	(Hz)	
19	Total doppler shift of reflected signal	(Hz)	
20	Latitude of specular point	(deg)	
21	Longitude of specular point	(deg)	
22	Speed of the specular point on the lunar surface	(M/sec)	
23	Vehicle look angles to earth	(deg)	
24			
25	(Euler angles of local horizon	(deg)	
26			
27			

Appendix IV (cont.)

3. Format Record 6 (all machine type Real) (cont.)

<u>Word No.</u>	<u>Contents</u>	<u>Units</u>
28	X } Spacecraft selenographic Y } unit velocity vector	(dim)
29		
30		
31	X } Selenographic unit vector Y } to earth	(dim)
32		
33		

The data frames are repeated each 6 records. The first data frame occupies records 2-7, the next 8-13, etc.

Note: Data do not always progress uniformly in time. Occasionally, data frames will reverse slightly in time for one frame, and then continue forward. This effect is caused by the sampling procedure in which a small deliberate overlap was inserted. Time ~~times~~ on data are correct.

tags

E. Definition of Contents

1. Data - the data have been defined under Subtasks 4 and 5 of the text.
2. Ephemeris and Ancillary Data - the formulae<sup>s</sup> used in computing trajectory related parameters are given in Appendix ~~6~~<sup>VI</sup>.

APOLLO 1-15, 16

Combined B.S. 170 140

71-008A-040

71-063C-140

72-021A-100

Appendix VI  
Integral Tape Format

The integral tape contains reduced data records generated in Subtasks 7, 8 and 9 (of Block Diagram I). This appendix gives the detailed formatting of ~~the~~<sup>one</sup> tapes and describes all ancillary computations.

A. Tape Organization

The table below gives the file contents <sup>AV</sup> and data record length for the integral tape.

<u>File No.</u>	<u>Contents</u>	<u>Record Length</u>
1	Apollo-14 116 cm	50 words
2	Apollo-14 13 cm	50 words
3	Apollo-15 116 cm	50 words
4	Apollo-15 13 cm	50 words
5	Apollo-16 116 cm	50 words
6	Apollo-16 13 cm	50 words

The tape is 9 track, 800 BPI, binary in XDS Sigma V machine images.

B. File Organization

1. Header Record
2. Data Record
3. :
4. (EOF) (End of File)
5. Header Record
6. :

- A - Alpha numeric
- I - Integer
- R - Real
- DPR - Double precision real

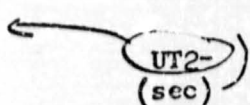
to bottom of next page

Appendix VI (cont.)

C. Header Record Format

<u>Word No.</u>	<u>Contents</u>	<u>Units</u>	<u>Machine Type</u> <sup>α</sup>
1/ 42	Alpha numeric File Identifier	--	A
43	Integer Day Number (Jan. 1 = 1)	(day)	I
44	Integer Year (GREGORIAN)	(year)	I
45 46	Double precision Julian ephermis day number at 00:00 GMT on day data were taken	(day)	DPR
47 48	Double precision Julian ephermis day of reference epoch	(day)	DPR
49	Time increment between data records	(sec)	R
50	Number of data records following this header record		I

D. Data Record Format (all machine type real)

<u>Word No.</u>	<u>Contents</u>	<u>Units</u>	
1	Data frame number from JM Doptrack tape		
2	Time data were taken: 	(sec)	
3	X } Components of selenographic unit position vector of spacecraft location	(dim)	
4			Y }
5			Z }
6	X } Components of selenographic velocity unit vector	(dim)	
7			Y }
8			Z }
9	Speed: Magnitude of spacecraft velocity vector (m/sec)		
10	X } Components of selenographic unit vector from center of the moon to center of the earth	(dim)	
11			Y }
12			Z }

Appendix VI (cont.)

D. Data Record Format (all machine type real) (cont.)

<u>Word No.</u>	<u>Contents</u>	<u>Units</u>	
13	X } Components of selenographic unit position Y } vector of specular Z } point location	(dim)	
14			
15			
16	θ } Euler angles of spacecraft attitude and ψ } local horizon frame φ }		
17			
18			
	$\bar{A}_{veh} = \begin{bmatrix} \phi \\ (x) \end{bmatrix} \begin{bmatrix} \psi \\ (z) \end{bmatrix} \begin{bmatrix} \theta \\ (y) \end{bmatrix} \begin{bmatrix} \bar{A}_1 \end{bmatrix}$ <p>(cw rotation looking in + axes direction)</p>		
19	α <sub>s</sub> } Vehicle look angles to specular point	(deg)	
20			
21	δ	Angle between plane of incidence and plane-containing vehicle x axis and direction vector to specular point	(deg)
22	α <sub>e</sub> } Vehicle look angles to earth	(deg)	
23			
24	Selenographic latitude of spacecraft position		(deg)
25	Selenographic longitude of spacecraft position		(deg)
26	Selenographic latitude of specular point		(deg)
27	Selenographic longitude of specular point		(deg)
28	Angle of incidence		(deg)
29	Instantaneous speed of specular point on lunar surface		(m/sec)
30	Predicted bandwidth for .1 radian rms surface slope		(Hz)
31	Difference between reflected and direct doppler shifts		(Hz)
32	Total doppler shift reflected signal		(Hz)

## Appendix VI (cont.)

## D. Data Record Format (all machine type real) (cont.)

<u>Word No.</u>	<u>Contents</u>	<u>Units</u>
33	Component of doppler shift due to earth's rotation	(Hz)
34	Altitude of spacecraft above lunar surface: Radius of center of the moon-1736 Km	(Km)
35	Normalized bistatic-radar cross-section	(dim)
36	Sigfac	(m <sup>2</sup> /w)
37	Polarized power	(arb)
38	Normalized polarized power	(°k)
39	Unpolarized power	(arb)
40	Normalized unpolarized power	(°k)
41	Equivalent area bandwidth	(Hz)
42	Normalized absolute moment bandwidth	(dim)
43	Normalized second moment bandwidth	(dim)
44	Centroid of the echo spectrum	(Hz)
45	RMS slopes inferred from equivalent area bandwidth	(deg)
46	Spare if value equals zero, otherwise handscaled one-half power echo bandwidths	(Hz)
47	Data validity flag	(-)
48	Spare if value = 0, otherwise value of spacecraft antenna gain in $\alpha_s, \beta_s$ , direction (cf Word No. 19, 20)	(dim)
49	Spare	(-)
50	Data record sequence number	(-)

**Note:** Data do not always progress uniformly in time. Occasionally, data records will reverse slightly in time for one record, and then continue forward. This effect is caused by the sampling procedure in which a small deliberate overlap was inserted. Time tags on data are correct. Overlapping data correspond to the same time interval but different sampling passes. Slight differences arise from variation in exact times averaged.

*not prepared*

## E. Data Parameter Definitions

The remainder of this section defines the contents of the data records just described above. The individual subsection numbers correspond to the word numbers in Section D (Data Record Format). If a particular quantity has been described at length elsewhere a reference will be given. Otherwise, the quantity is defined here.

1. Frame Number - identifies the JM Doptrack tape frame number corresponding to the Integral tape record number.
2. Time - gives the UT2 at which the data were taken. This time corresponds to the mid-point of the averaging interval, as described under Subtask 4. All trajectory parameters have been interpolated to this time, so that geometrical quantities corresponds to the location of the specular point on the mean lunar surface at the middle of the averaging interval.
- 3, 4, 5. Selenographic Unit Position Vector - is defined with respect to the lunar surface. This vector is a unit vector directed from the center of the moon for the instantaneous location of the spacecraft. The X, Y, Z directions are defined as follows:
  - X = Mean Earth direction
  - Y = Mean direction of the following limb
  - Z = North polar directionThe selenographic coordinants are obtained by rotation from the selenocentric geoequatorial units of the epoch given in the Header Record. Procedures are described elsewhere (Tyler, 1968).
- 6, 7, 8. Selenographic Unit Velocity Vector is a unit vector in the direction of the spacecraft velocity. The coordinant system is the same as that given in items 3, 4, 5 above.
9. Speed - is the magnitude of the spacecraft velocity vector.
- 10, 11, 12. Selenographic Unit Vector to Earth - is a unit vector giving the direction from the lunar center of mass to the center of mass to the earth in the selenographic coordinant system described in the 3, 4, 5 above.

- 13, 14, 15. Selenographic Unit Position Vector of Specular Point - is a unit vector from the center of mass of the moon to the location of the specular point on the mean spherical lunar surface. For this computation the lunar radius is taken as 1736 km. The specular point is the location on the mean lunar surface where the angles of incidence and reflection are equal (cf Tyler, [1963]).
- 16, 17, 18. Euler Angles of Spacecraft Attitude - connect the spacecraft attitude with a local horizon reference frame. Both the local horizon and the Euler angles are defined in Appendix IX.
- 19, 20. Look Angles to Specular Point - are the vehicle polar coordinance. These quantities are defined in Appendix IX.
21. Plane of the Vehicle - orientation with respect to the plane of incidence is given by the angle  $\delta$ . This quantity is necessary to define the vehicle attitude with respect to the plane incidence. The angle  $\delta$  is defined in Appendix IX.
- 22, 23. Look Angles to Earth - are the vehicle polar coordinance of a unit vector in the earth center of mass direction. These quantities are computed in the same manner as item 19, 20 above using the unit vector to earth.
24. Selenographic Latitude of Spacecraft Position - is the selenographic latitude of the sub-spacecraft point computed from the Z component unit vector given in items 3, 4, 5.
25. Selenographic Longitude of Spacecraft Position - is the selenographic longitude of the spacecraft of the sub-spacecraft position computed from item 3, 4, 5 according to astrometric convention, western limb of the moon leading.
26. Selenographic Latitude of Specular Point - is the selenographic latitude of the specular point on a mean spherical lunar surface computed from item 15.
27. Selenographic Longitude of Specular Point - is the selenographic longitude of the specular point on the mean spherical lunar surface computed from items 13, 14, 15.

28. Angle of Incidence - is the angle of incidence on mean spherical lunar surface at the specular point (cf Tyler, 1968).
29. Speed of the Specular Point - is the speed with which the instantaneous specular point moves across the mean lunar surface (Tyler, 1968).
30. Predicted Bandwidth - is the one half spectral width predicted for a 0.1 radian rms surface slope, based on the instantaneous angle of incidence and specular point velocity. Computation is after Fjeldbo (1964), also described in Tyler (1968). Fjeldbo gives a theoretical expression for the 1/2 power echo bandwidth

$$\Delta f = 4(2 \ln 2)^{1/2} \frac{v_s}{\lambda} \frac{h_o}{d_o} \cos \phi$$

where  $\phi_s$  = velocity of the specular point on the mean lunar surface,  $\lambda$  = wavelength of the radiation (either 116 cm or 13 cm),  $\phi$  = angle of incidence at the specular point, and the quantity  $\frac{h_o}{d_o}$  = the mean lunar rms slope.

The quantity  $\Delta f$  is the 1/2 power bandwidth predicted for gaussian spectrum. Such a spectrum would result from a gently undulating surface with gaussian autocorrelation function.

31. Difference Between Reflected and Direct Doppler Shifts - is the predicted frequency difference between a wave reflected from the specular point and the signal traveling directly from the spacecraft to earth. Sign convention is such that the difference is positive for a reflected doppler shift greater than that of the direct doppler shift.
32. Doppler Shift - is the total doppler shift expected from the reflected signal. Computation of this doppler shift includes spacecraft motion and the earth's rotation, but does not include the rate of change of distance between the earth and the moon.
33. Doppler due to Earth's Rotation - is the component of the doppler shift for a signal arriving from the direction of the moon due to the earth's rotation.

Appendix VI (cont.)

34. Altitude - of the spacecraft above the lunar surface has been computed assuming a lunar radius equal to 1736 km. The magnitude of the spacecraft radius vector from the lunar center of mass is obtained by adding the contents of word no. 34 to 1736 km.
35. Normalized Bistatic-Radar Cross-Section - is the bistatic-radar cross-section of a smooth conducting sphere of the same radius and relative geometry as the moon. Following Fjeldbo (1964) this cross-section is given by

$$\sigma_B = \frac{4\pi R_1^2 \cos \phi}{\left(\cos \phi + \frac{2d_{or}}{R}\right) \left(1 + \frac{2d_{or} \cos \phi}{R}\right)}$$

where

$R_1$  = distance from transmitter to the center of the moon

$R$  = lunar radius ( $1.736 \times 10^6$  m)

$\phi$  = angle of incidence (cf item 28)

$d_{or}$  = distance from the transmitter to the specular point on the mean lunar surface.

36. Sigfac - is a multiplicative constant relating instantaneous geometry and received power to surface reflectivity.

$$\text{SIGFAC} = \frac{(4\pi)^2 R_1^2 R_2^2}{A P_T G_T \sigma_B}$$

where

$R_1$  = distance from transmitter to center of the moon

$R_2$  = distance from receiving site to center of the moon

$A$  = effective aperture of receiving antenna

$P_T$  = transmitted power

$G_T$  = transmitting antenna gain in specular point direction

$\sigma_B$  = bistatic-radar cross-section for a perfectly conducting moon

For convenience, this expression is evaluated with the following numerical values for the quantities above:

Appendix VI (cont.)

$R_1$  = instantaneous value from MSC trajectory

$\sigma_B$  = instantaneous value from item 35 above

$R_2 = 4 \times 10^8$  m

$A = 0.5 (22.5)^2 \pi$

$G_T = 1$

$P_T = .2.5$  w

These values give only order of magnitude results for this experiment.

37. Polarized Power - is the experimenter's best estimate of the polarized component of the received echo total power. Extraction of the polarized power is discussed elsewhere (cf Subtask 8).

Denote the polarized power spectrum  $P_p(k)$ . Consider the figure below. Polarized power is determined from

$$P = \sum_{k=B_1}^{B_2} (P_p(k) - n)$$

The  $P_p(k)$  is a polarized power spectrum. In the determination of  $P$ , the signal limits  $B_1$ ,  $B_2$  and  $n$  are selected by the experimenter. The quantity  $n$  is chosen on the basis of

$$\sum_{B_1'}^{B_2'} (P_p(k) - \hat{n}) \sim 0$$

where  $B_1'$ ,  $B_2'$  represent spectral limits containing no echo signal, and  $\hat{n}$  represents a sequence of trials of  $n$ . The limits  $B_1$ ,  $B_2$ ,  $B_1'$ ,  $B_2'$  are varied as is necessary to follow the changing echo signal.

38. Normalized Polarized Power - the quantity contained in item 37 divided by the average power spectral density of the system noise level. This quantity has been discussed in detail elsewhere (cf Subtask 3).

Using the notation introduced under item 37,

$$\text{Normalized Polarized Power} = P/n$$

where P and n have the same meaning as above.

Note: P/n is extremely sensitive to the choice of n. Thus, polarized power is considered the best overall measure of received polarized echo power. But, P/n provides the only method, through the measure of system temperature, of obtaining an absolute power calibration. Similarly, the value of n may be determined from the ratio of polarized power to P/n, so that the variations and system temperature and/or gain may be estimated.

39. Unpolarized Power - is the analogous quantity to item 37, for the unpolarized power spectrum. The unpolarized power is obtained in a manner similar to that used to compute polarized power. Letting

Appendix VI (cont.)

$P_u(k)$  represent the unpolarized power spectra, and referring to the figure below, the unpolarized power is given by

$$U = \sum_{\tilde{B}_1}^{\tilde{B}_2} (P_u(k) - \tilde{n})$$

where the tilda's refer to the values of B and n used in the unpolarized power spectrum. In general, the limits for the polarized and unpolarized echoes will be different, as will the value of the system noise level. The difference in frequency limits arises from the difference in the spectral distribution of the unpolarized power; the difference in system noise temperature arises from the signal processing used to separate these quantities (cf Subtask 4, 5). The value of  $\tilde{n}$  is chosen in a manner similar to that of n in item 37. In some cases, it is not clear that all the unpolarized power is contained in the receiver passband. In this event,  $\tilde{B}_1$  or  $\tilde{B}_2$  is set equal to the upper or lower frequency limit as appropriate.

40. Normalized Unpolarized Power - is the analogous quantity to item 38, for the unpolarized power spectrum. The normalized unpolarized power is defined as

$$\text{Normalized Unpolarized Power} = U/\bar{n}$$

where the symbols have the same meaning as in item 39. Comments given under item 38 are also germane to normalized unpolarized power.

41. Equivalent Area Bandwidth - the spectrum of a bistatic-radar echo from a well behaved surface may be written as (Fjeldbo, 1964).

$$S(f) = e^{-\pi f^2 \left[ 4v_s (\pi/\lambda) \cos \phi \left( \frac{h_o}{d_o} \right) \right]^2} = e^{-f^2/2\sigma^2}$$

where

$f$  = frequency measured from the centroid of the echo spectrum

$v_s$  = speed of the specular point across the mean lunar surface

$\lambda$  = wavelength

$\phi$  = angle of incidence, and

$h_o/d_o$  = rms slope

\*The three machine calculated bandwidths, i.e., the equivalent area bandwidth, the absolute moment bandwidth, and the second moment bandwidth, provide three quasi-independent methods of determining the spectral width of the received echoes. The equivalent area bandwidth provides a standard result that is not particularly sensitive to the gaussian, or non-gaussian nature of the echo spectrum. The absolute moment bandwidth and the second moment bandwidth so emphasize departures from gaussian because of the increasing importance given to the wings of the spectrum.

Equivalent area bandwidths have been used to determine lunar rms slopes. The absolute moment bandwidths and the second moment bandwidths, when normalized by the equivalent area bandwidth, give a sensitive measure of the departures of the echo spectra from the gaussian conditions. RMS slopes derived from these measures are termed "gaussian equivalent slopes" in that they would correspond to true surface conditions for a surface with gaussian statistics and a gaussian autocorrelation function with the same equivalent widths. A more complete description of the lunar slopes requires additional analysis (e.g., see Parker and Tyler, 1973).

Solving for rms slope in terms of measured values of standard deviation,  $\hat{\sigma}$ , of an experimental spectrum yields

$$h_o/d_o = \frac{\hat{\sigma}}{2(v_s/\lambda) \cos \phi}$$

Thus, the rms slope may be readily determined from a experimental curve in terms of the  $e^{-1}$  width of that curve. The equivalent area bandwidth is a measure of  $\hat{\sigma}$  based on an equivalent rectangular spectrum of the same area as the experimental spectrum. This width is computed as

$$\hat{\sigma}_{ea} = \frac{\sum_{k=C_1}^{C_2} F_p(k)}{\max P_p(k)} \cdot (2\pi)^{-1/2}$$

$$C_1 < k < C_2$$

Referring to the figure which follows, the quantity  $\hat{\sigma}_{ea} = \sigma$  if the observed curve is gaussian and noiseless. For non-gaussian data  $\hat{\sigma}_{ea}$  is still a measure of the bandwidth, albeit the interpretation must be modified. rms slopes determined from  $\hat{\sigma}_{ea}$  and expression above will be referred to as equivalent area slopes. The quantity  $\hat{\sigma}_{ea}$  is the equivalent area bandwidth.

4.2. Normalized Absolute Moment Bandwidths - are based on an equivalent value of  $\hat{\sigma}$  computed from the absolute moment of the data. That is,

$$\hat{\sigma}_{am} = \frac{\sum_{k=C_1}^{C_2} P_p(k) |k-\bar{k}|}{\sum_{k=C_1}^{C_2} P_p(k)} \cdot \sqrt{\frac{\pi}{2}} ; \quad \bar{k} = \frac{\sum_{k=C_1}^{C_2} P_p(k) k}{\sum_{k=C_1}^{C_2} P_p(k)}$$

for a gaussian spectrum the equivalent area moments and the absolute moments will be equal

$$\hat{\sigma}_{am} = \hat{\sigma}_{ea} = \sigma$$

where the symbols have the same meaning as in item 41.

The normalized absolute moment bandwidth is

$$\hat{\sigma}_{am} / \hat{\sigma}_{ea}$$

For a gaussian echo spectrum this ratio will be unity.

43. Normalized Second Moment Bandwidth - the second moment bandwidth is also based on gaussian equivalence. This bandwidth is defined as

$$\hat{\sigma}_{sm} = \frac{\sum_{k=C_1}^{C_2} P_p(k) (k-\bar{k})^2}{\sum_{k=C_1}^{C_2} P_p(k)}; \quad \bar{k} = \frac{\sum_{k=C_1}^{C_2} P_p(k) \cdot k}{\sum_{k=C_1}^{C_2} P_p(k)}$$

Again, for a gaussian echo spectrum

$$\hat{\sigma}_{sm} = \hat{\sigma}_{am} = \hat{\sigma}_{ea} = \sigma$$

where the symbols have the same meaning under items 42 and 41.

The normalized second moment bandwidth is given by

$$\hat{\sigma}_{sm} / \hat{\sigma}_{ea}$$

Again, departures of this ratio from unity are indicative of a non-gaussian received echo spectrum

44. Centroid of the Echo Spectrum - the centroid of the echo spectra are defined in the standard way

$$\bar{k} = \frac{\sum_{k=C_1}^{C_2} P_p(k) \cdot k}{\sum_{k=C_1}^{C_2} P_p(k)}$$

where the symbols have the same meaning as in 41, 42 and 43. The values of  $C_1$ ,  $C_2$  are held constant throughout items 41, 42, 43 and 44. The echo spectrum centroid is used in the computations of the absolute moment bandwidths and the second moment bandwidths. It is also useful for estimation of the observed doppler difference (cf item 31). However, the centroid has no direct meaning in an

absolute sense in that the transmitter frequencies from the spacecraft are not known precisely.

45. rms Slopes - are obtained from the equivalent area bandwidths according to

$$\frac{h_o}{d_o} = \frac{\hat{\sigma}_{ea}}{2(v_s/\lambda) \cos \phi}$$

and

$$\text{rms slope} = \tan^{-1} (h_o/d_o)$$

where the results are expressed in degrees for convenience. The quantities  $v_s$ ,  $\lambda$ ,  $\phi$  and  $\hat{\sigma}_{ea}$  have been defined in item 41.

46. Handscaled 1/2 Power Echo Bandwidths - handscaling of polarized echo bandwidths has been discussed previously under Subtask 10. A 1/2 power echo bandwidth is defined by the quantity "B" in the figure which follows. In practice, this value is obtained by handscaling data from plots. The handscale bandwidths provide a rapid, simple technique for the evaluation of lunar rms surface slopes. The handscaled bandwidths were also used as a controlling parameter in development of automated techniques for obtaining echo bandwidths. rms slopes may be obtained from the handscaled bandwidths by

$$\text{rms slope} = 5.7^{\circ} \times B / (\text{predicted } 1/2 \text{ power bandwidth for } 0.1 \text{ rms slopes})$$

As before, in item 45, the result is given in degrees for convenience. Predicted 1/2 power bandwidths for 0.1 rms slopes are given in Word No. 30 of the integral tape data records (cf item 30).

47. Flag - the flag word contains a seven level binary code that indicates data quality. A bit in the "1" condition indicates the existence of a special condition in the data. A bit position in the "0" state carries no meaning other than that the data are normal.

The interpretation of the bit positions is as given below.

<u>Bit in "1" Condition</u>	<u>Implication</u>
1	Polarized power data questionable or no good
2	Unpolarized power data questionable or no good
3	Polarized noise level, $n$ , (cf item 37) changed this data record
4	Polarized integration bounds $B_1, B_2$ , (cf item 37) changed this data record
5	Unpolarized noise level, $\tilde{n}$ , (cf item 39) changed this data record
6	Unpolarized integration bounds, $\tilde{B}_1, \tilde{B}_2$ , (cf item 39) changed this data record
7	System gain changed this data record

Explanation

Bit Position "1"

Polarized data may be flagged for any one of a number of reasons. The presence of interference, an error in setting the integration bounds, or a tape drive error in the data processing are examples of difficulties that would result in such a flag. In case of gross errors the flag represents an objectively known bad data point. In the case of more subtle phenomena such as interference, the flag represents an experimenters subjective opinion. For the 116 cm data interference is the predominant cause of a data bad flags. Data users who wish to examine this question for themselves may do so by reprocessing the data from the JM Doptrack tapes, however, it is very strongly recommended that no flagged data be used without taking this precaution.

Bit Position "2"

Unpolarized data may be flagged for the same reasons as those given for the polarized data under bit position "1" above. However, because gross errors for polarized and unpolarized data may be independent, and because the unpolarized data possess a certain immunity to interference, which tends to be polarized, the flags in bit position "1" and "2" are not necessarily coincident. As before, in the case of interference, the investigator's judgment is involved.

Bit Position "3"

This flag is set when the noise level, i.e., n in item 37 is changed during the data reduction process. This flag serves to alert the user that such a change has been made. Any discontinuity that occurs when this bit is set is likely to result from this cause. In the case of the polarized power such discontinuities are generally quite small, on the order of 1%. However, in the case of the normalized polarized power such discontinuities may be large, on the order of two. Obviously, no physical significance should be attached to such discontinuities.

Bit Position "4"

Changes in the integration bounds are flagged for reasons similar to those given under bit position "3". The bounds,  $B_1$ ,  $B_2$ , vary with the changing width and location of the polarized echo. Usually, such changes are very small and their effect is not noticeable in the data.

Bit Position "5"

Changes in the unpolarized noise level,  $\tilde{n}$ , are made for the same reasons as those described under bit position "3". As before, changes in the unpolarized power, and especially the normalized unpolarized power, that occur with these changes in  $\tilde{n}$  are non-physical.

Bit Position "6"

The comments that apply to the polarized integration bounds given under bit position "4" also apply here.

Bit Position "7"

System gain changes may occur during data reception in the receiving systems or during data playback in the record reproduction system. Such changes are flagged since they will appear as a change in the polarized and unpolarized signal levels. Gain changes do not affect measures of echo bandwidths.

48. Antenna Gain - is the gain of the spacecraft antenna in the  $\alpha_s, \beta_s$  direction determined from *this needs completing*

*There is 49?*

Stanford Apollo Bistatic-Radar Experiment (S-170):  
National Space Science Data Center Data Description

G. L. Tyler  
H. T. Howard  
G. R. Dow

February 15, 1973

Technical Report No. 3282-1

Prepared under  
National Aeronautics and Space Administration  
Contract NAS 9-10579

**CENTER FOR RADAR ASTRONOMY  
RADIOSCIENCE LABORATORY**

**STANFORD ELECTRONICS LABORATORIES**

**STANFORD UNIVERSITY • STANFORD, CALIFORNIA**



STANFORD APOLLO BISTATIC-RADAR EXPERIMENT (S-170):  
NATIONAL SPACE SCIENCE DATA CENTER DATA DESCRIPTION

February 15, 1973

G. L. Tyler  
H. T. Howard  
G. R. Dow

Technical Report No. 3282-1

Prepared under  
National Aeronautics and Space Administration  
Contract NAS 9-10579

Center for Radar Astronomy  
Stanford University  
Stanford, California 94305

## Contents

Introduction. . . . .	1
Synopsis of Observations. . . . .	4
Data Collection, Processing, Reduction. . . . .	6
Subtask 1	
Data Collection. . . . .	9
Subtask 2	
Sampling . . . . .	11
Subtask 3	
Conversion to Frequency Domain . . . . .	12
Subtask 4	
Generation of Coherency Matrix . . . . .	13
Subtask 5	
Correction for System Polarization Parameters. . . . .	16
Subtask 6	
Merging Observations with Trajectory . . . . .	21
Subtask 7	
Computation of Polarized and Unpolarized Parts, Carrier Suppression. . . . .	23
Subtask 8	
Computation of Total Received Power, Echo Moments. . . . .	24
Subtask 9	
Final Editing of Data. . . . .	26
Subtask 10	
Displaying, Scaling, and Copying the Data. . . . .	28
Subtask 11	
Utility Routines . . . . .	29
Appendix I	
VHF Receiver . . . . .	30
Appendix II	
S-Band Receiver. . . . .	31
Appendix III	
Apollo Bistatic-Radar Receiving System 116 cm Uncorrected Frequency Response . . . . .	32
Apollo Bistatic-Radar Receiving System 13 cm Uncorrected Frequency Response . . . . .	33
Appendix IV	
JM Doptrack Tape Format . . . . .	34
Appendix V	
Carrier Suppression Algorithm. . . . .	39
Appendix VI	
Integral Tape Format . . . . .	43

Appendix VII	
Cross-Reference Table for JM Doptrack/Integral Tape Trajectory Parameters. . . . .	62
Appendix VIII	
Matrix Correction Factors. . . . .	64
Appendix IX	
Coordinate Transformations . . . . .	66
Appendix X	
Relationship Between the Coherency Matrix and Other Specifications of Polarization . . . . .	73
Appendix XI	
XDS Sigma 5 Machine Images . . . . .	77
References. . . . .	79
Notes . . . . .	81

## Introduction

The Stanford Apollo Bistatic-Radar Experiment (S-170) was carried out during the lunar orbit phase of the Apollo 14, 15, and 16 flights. The experiment was unique in that no special equipment was placed onboard the Apollo vehicles and carried to the moon, and that the principal observations were carried out on the ground. Radio-frequency transmissions from the orbiting command-service-module were directed toward the moon and received on the earth after reflection from the lunar surface. Two wavelengths, 13 cm (2287.5 MHz, S-band) and 116 cm (259.7 MHz, VHF), were used. The best data were obtained during periods when the spacecraft was maneuvered to maintain a predetermined, although changing, attitude with respect to the earth and moon. During these periods, data were obtained at the two wavelengths simultaneously. Data were also obtained at the 116 cm wavelength during periods of inertial hold and SIM bay attitude maneuvers. Data reception took place at two sites on the earth, the NASA-DSN 64 m antenna facility located near Barstow, California and the Stanford Research Institute/Stanford University 46 m antenna facility located on the campus of Stanford University, Stanford, California. The NASA facility was used for reception of the 13 cm data, the Stanford facility for the 116 cm data. In both cases the elements of the receiving system critical to the experimental objectives were under direct control of the experimenters. At the DSN, a Signal Conditioning Unit designed and constructed at Stanford was inserted as a critical series element in the data receiving system and used to set system bandwidths, levels and timing information for the analog recording system. Input signal levels, bandwidths, and

frequencies to the Signal Conditioning Unit from the DSN were specified and monitored in real-time during data collection by the experimenters. Data reduction was carried out at the Stanford Sigma 5 Real-Time Computation Facility. With two exceptions (cf. Notes on Block Diagram I, 4d, and Appendix V) identical programs and procedures were used for 13 cm and 116 cm data. Also, with one exception, the same programs were used for all three flights (cf. Subtask 2). However, certain parameters, defined elsewhere in the report, were varied for data at the two wavelengths.

Good data were obtained from the three flights. In the data sets accompanying this report we include the simultaneous 13 cm and 116 cm observations, but not the 116 cm data obtained in the inertial hold and SIM bay attitudes. Data are given in two forms:

- a) A complete set of observations reduced to short time averages of the electromagnetic wave spectra for the 13 cm and 116 cm observations. These observations have been corrected for instrumental effects, and are unedited. Tapes containing these data are referred to as JM Doptrack tapes. The observations have been merged with trajectory data obtained from the Manned Space Flight Center in Houston, and certain ancillary data computed from the trajectory.
- b) A complete set of reduced data records, called Integral tapes, obtained from the JM Doptrack tapes, which describe certain properties of the JM Doptrack data, such as moments of the echo spectra, and inferred properties of the lunar surface, such as rms slopes.

There is one-to-one correspondence between the Integral data and the JM Doptrack data; an interested investigator may use either the reduced data records given on the Integral tapes, or use the JM Doptrack tapes to verify the reduction procedure and perform additional reductions.

The remainder of this report describes the data collection and reduction system in some detail, attempts to give cautioning notes to

the data user, and describes the tape contents and formats for JM Dop-track and Integral tapes. However, no particular attempt to explain the motivation for the overall data reduction procedures will be made, except as it affects individual steps not described elsewhere. A more general understanding of the experiment, its goals, limitations, and preliminary results may be obtained from the references listed below:

Howard, H. T. and G. L. Tyler, "Bistatic-Radar Studies of the Lunar Surface," Apollo 14 Preliminary Science Report, NASA publication SP-272, 1971.

Howard, H. T. and G. L. Tyler, "Bistatic-Radar Investigation," Apollo 15 Preliminary Science Report, NASA publication SP-289, p. 23-1, 1972.

Howard, H. T. and G. L. Tyler, Apollo 16 Preliminary Science Report, NASA publication SP-315, p. 25-1, November, 1972.

Tyler, G. L. and H. T. Howard, "Bistatic Radar Observations of the Lunar Surface with Apollos 14 and 15," paper presented at Third Lunar Science Conference, Houston, Texas, January, 1972.

Tyler, G. L. and D. H. H. Ingalls, "Functional Dependence of Bistatic Radar Frequency Spectra on Lunar Scattering Laws," J. Geophys. Res., Vol. 76, No. 20, pp. 4775-4785, July, 1971.

## Synopsis of Observations

A synopsis of the observations included with this report is given in Table I, "Stanford Apollo Bistatic-Radar Experiment Parameters." The definitions of the columns in Table I are given below:

SPACECRAFT - Designation of flight number

ORBIT - NASA-MSO orbit numbers, counted from lunar orbit insertion

WAVELENGTH - Either 13 cm or 116 cm, wavelength of electromagnetic radiation from command-service-module, corresponds to frequencies 2287.5 MHz and 259.7 MHz respectively.

ANTENNA - Command-service-module antenna in use. Quantities in ( ) are NASA-MSO designation. Antenna patterns used in data reduction obtained from NAA (1966a, 1966b, 1969), and MEC (1967). Apollo 14 experiment required compromise in spacecraft attitude to accommodate patterns from two fixed antennas.

3 db BEAMWIDTH - One-half power antenna beamwidths

POLARIZATION - Of command-service-module antenna

GAIN - Command-service-module antenna gain

POWER - Transmitted power, from command-service-module

SYSTEM TEMPERATURE - Equivalent temperature of receiving system on the earth, looking at cosmic background radiation perpendicular to plane of galaxy.

TABLE I

## Stanford Apollo Bistatic-Radar Experiment Parameters

SPACECRAFT	ORBIT	WAVELENGTH	ANTENNA	3 db BEAMWIDTH	POLARIZATION	GAIN <sup>β</sup>	POWER <sup>γ</sup>	SYSTEM TEMPERATURE <sup>δ</sup>
Apollo 14	25	13 cm	Cavity backed helix (OMNI <u>C</u> )	~60°	Right elliptical axial ratio ~7 db	-1.5 db	~4 W	27°K ± 3°
Apollo 14	25	116 cm	Scimitar (VHF <u>LEFT</u> )	α	Linear, maintained in plane of incidence	~0 db	~2.5 W	~1000°K ± 50°
Apollo 15	28	13 cm	Steerable crossed dipoles (HIGH GAIN, <u>WIDE</u> )	~40°	Right circular axial ratio <math>\leq 1.0</math> db	-1.5 db	~4 W	27°K ± 3°
Apollo 15	28	116 cm	Scimitar (VHF <u>RIGHT</u> )	α	Linear, varies with respect to plane of incidence	~0 db	~2.5 W	~1000°K ± 50°
Apollo 16	40	13 cm	Steerable crossed dipoles (HIGH GAIN, <u>WIDE</u> )	~40°	Right circular axial ratio <math>\leq 1.0</math> db	-1.5 db	~4 W	27°K ± 3°
Apollo 16	40	116 cm	Scimitar (VHF <u>LEFT</u> )	α	Linear, maintained in plane of incidence	~0 db	~2.5 W	~1000°K ± 50°

α beamwidth of scimitar not defined

β includes circuit losses, nominal values ± 3 db

γ in carrier signal, nominal values, actual values not measured in flight

δ varies with orbital position of spacecraft, cold sky values given

## Data Collection, Processing, Reduction

Block Diagram I, located at the rear of the report, depicts the flow of data through collection, processing, and reduction. Annotations and notes (circled numbers) give brief comments or descriptive titles as guides for reference. The overall data flow is divided into 11 subtasks, indicated by horizontal brackets. The remainder of the report is subdivided according to the subtasks. It is assumed that the reader has general familiarity with analog-to-digital and digital techniques for data reduction and analysis. Critical data reduction parameters are given in Table II and antenna parameters are given in Tables III and IV.

Each subtask description provides a general explanation of that subtask function. An attempt has been made to maintain independent description, with minimum reference to other functions. Highly technical details, such as magnetic tape formats and coordinate descriptions, are reserved for the appendixes. In this way a careful reading of the subtask descriptions, in connection with Block Diagram I, should provide a good overview of the data reduction process. The appendixes may be read at a later time, or for details.

A THOROUGH STUDY OF BLOCK DIAGRAM I PRIOR TO THE USE OF REPOSITORY DATA IS VERY HIGHLY RECOMMENDED.

TABLE II

## STANFORD APOLLO DUAL-FREQUENCY BISTATIC-RADAR DATA SUMMARY

	APOLLO 14		APOLLO 15		APOLLO 16	
	116 cm (VHF)	13 cm (S-BAND)	116 cm (VHF)	13 cm (S-BAND)	116 cm (VHF)	13 cm (S-BAND)
Julian Ephemeris Day (00:00 UT2 Preceding Data)	2440988.4		2441164.5		2441430.5	
Reference Epoch for Coordinate Systems	2440952.509		2441317.752		2441317.752	
CALENDAR DATE	February 6, 1971		August 1, 1971		April 23, 1972	
Orbit Number(From Lunar Orbit Insertion)	25		26		40	
Transmitter Frequency	259.7 MHz	2287.5 MHz	259.7 MHz	2287.5 MHz	259.7 MHz	2287.5 MHz
UT2 START/STOP TIME	06:37:17/07:30:34	06:38:30/07:32:28	01:23:00/02:23:58	01:16:30/02:29:00	01:16:30/02:16:26	01:17:00/02:27:05
Spacecraft Antenna (MSC Designation) High Gain Antenna Pointing Angles	VHF <u>LEFT</u>	OMNI <u>C</u>	VHF <u>RIGHT</u>	HIGH GAIN ( <u>WIDE</u> )	VHF <u>LEFT</u>	HIGH GAIN ( <u>WIDE</u> )
$\alpha$	-	-	-	144. <sup>o</sup>	-	145. <sup>o</sup>
$\beta$	-	-	-	122. <sup>o</sup>	-	302. <sup>o</sup>
Data Source	Stanford 10.003 MHz i.f. rcvr	DSN/STANFORD Closed Loop rcvr	Stanford 10.003 MHz i.f. rcvr	DSN/STANFORD Closed Loop rcvr	Stanford 10.003 MHz i.f. rcvr	DSN/STANFORD Closed Loop rcvr
Receiver Bandwidth	~3.5 kHz	~20.0 kHz	~3.5 kHz	~20.0 kHz	~3.5 kHz	~20.0 kHz
Data Sampling Frequency	10.0 kHz	43.0 kHz	10.0 kHz	43.0 kHz	10.0 kHz	43.0 kHz
Total Analysis Band- width	5.0 kHz	21.5 kHz	5.0 kHz	21.5 kHz	5.0 kHz	21.5 kHz
N, Number of Analysis Bin	1024	1024	2048	1024	2048	1024
Analysis Resolutior	9.8 Hz	42.0 Hz	4.9 Hz	42.0 Hz	4.9 Hz	42.0 Hz
Length of Data Window/Transform	0.1024 sec.	0.02381395 sec.	0.2048 sec.	0.02381395 sec.	0.2048 sec.	0.02381395 sec.
L, Number of Transforms Averaged per JM Record (see Subtask 4)	26	100	23	99	23	99
Frame Length	2.6624 sec.	2.381395 sec.	4.7104 sec.	2.357581 sec.	4.7104 sec.	2.357581 sec.

TABLE III

Stanford Research Institute 46 m Antenna Performance (116 cm)

Aperture	Efficiency	Feed System	Mount	Pointing Loss
46 m dia.	$\sim 35\% \pm 5\%$	Crossed dipole array axial ratio $\sim 1. \text{ db} \pm 0.5^\alpha$ isolation $\sim 16 \text{ db} \pm 1.0$	el/az	$< 0.1 \text{ db}$

TABLE IV

NASA DSN 64 m Antenna Performance (13 cm)\*

Aperture	Efficiency	Feed System	Mount	Pointing Loss
64 m dia.	$58\% \pm 4\%$	Waveguide horn axial ratios $\gtrsim 0.8 \text{ db}^\beta$ isolation $\gtrsim 26 \text{ db}^\gamma$	el/az	$< 0.03 \text{ db}$

---

$\alpha$  estimated

$\left. \begin{matrix} \beta \\ \gamma \end{matrix} \right\}$  Private communication, D. Bathker, JPL, 1973.

\* DSN, 1972

## Subtask 1

### Data Collection

- a) 116 cm. A detailed block diagram of the 116 cm receiver is given in Appendix I. The receiver is a superheterodyne of standard design. An unusual feature of this system is the summed second local oscillator signal used to produce offset 9.0 and 10.003 MHz intermediate frequency signals. In operation, the 10.003 MHz channel was tuned to the downlink signal carrier and its accompanying echo, while the 9.0 MHz channel was tuned to the subcarrier signal displaced  $\pm 31.6$  KHz from the 259.7 MHz carrier. This procedure was adopted to provide frequency dispersive redundancy against locally generated interference at the main carrier frequency. The receiver passband characteristics are given in Appendix III. However, all data given here were obtained through the main 10 MHz channel. Receiver outputs were multiplexed with standard frequency references and clock signals and recorded on analog tape. Parameters of the Stanford Research Institute 46 m dish are given in Table III.
- (b) 13 cm. A detailed block diagram of the 64 m 13 cm receiving system is given in Appendix II. Again, standard superheterodyne techniques are employed. All 13 cm data were obtained from a phase-locked loop signal tracking system using manual tracking when the direct signal dropped below threshold of the phase-locked loop. The receiver passband characteristics are given in Appendix III. The NASA-DSN station configuration for this experiment is given elsewhere (DSN, 1970, 1971). Again, analog signals from the receiver output multiplexed with clock and reference frequencies were recorded. Parameters of the NASA DSN 64 m dish are given in Table IV.

Subtask 1 (cont.)

(c) Critical Bandwidths. Appendix III gives the power spectral densities obtained at the receiver outputs for the three Apollo experiments with uniform power spectrum (white) noise input. These curves were obtained in Subtask 4, and were used in the data normalization. For the 116 cm system additional checks made with coherent signals within  $\pm 5$  MHz either side of the 10 MHz intermediate frequency and within  $\pm 20$  MHz of the first intermediate frequency verified the absence of spurious responses that would not be detected by the noise calibration technique. Similar tests have been carried out by the DSN and the experimenters at the 64 m facility. Thus, the curves in Appendix III accurately represent the receiver response to signals near the frequency to which the receivers were tuned. Image rejection in the 116 cm system was greater than 100 db.

## Subtask 2

### Sampling

Data sampling was carried out using standard techniques on the Stanford Sigma 5 Real-Time Computation Facility. Right circular and left circular polarization signal channels were sampled simultaneously in synchronism with the multiplexed time reference signals. Sampling was initiated at the start of an even 10 sec. interval (UT2) by a start pulse derived from the recorded time code. The sampling programs were improved between the Apollo 15 and 16 experiments to obtain higher playback rates for the 13 cm data (see Block Diagram I, Notes, 4d). With this exception, the same computer programs were used for data reduction from the three sets of observations. A small overlap was provided between subsequent sample data tapes. These overlaps were carried through the remainder of the data processing. Tape recorder playback levels were adjusted for equality between left circular and right circular polarization using the controlled reference signal levels for calibration. The playback recorder electronics were equalized for the particular tape source (FR1400 A, FR1400 B, HP3955B) prior to sampling data from that source. Output from the data sampling process was stored on magnetic tape. The quantization level was 8 bits. The  $i^{\text{th}}$  data sample generally will be denoted  $\hat{d}_i$ : data from the left circularly polarized antenna  $1\hat{d}_i$ , data from the right circularly polarized antenna  $2\hat{d}_i$ .

### Subtask 3

#### Conversion to Frequency Domain

All data have been rendered in the frequency domain in the form of modified complex Fourier coefficients (Blackman and Tukey, 1958). A sequence of data samples was multiplicatively weighted with a sine-squared (Hanning) data window and then Fourier analyzed using fast Fourier transform techniques. Analytically, the data samples were grouped, separately for each polarization, according to

$$d_j^n = \hat{d}_i, \quad (1)$$

where  $i = nN + j$ ,  $j \leq N$ ;  $n, N, j$  positive integers or zero. The modified complex Fourier coefficients are

$$f_k^n = \sum_{j=0}^{N-1} \sin^2 \left( \frac{2\pi}{N} j + \frac{\pi}{N} \right) d_j^n e^{-i(2\pi/N)jk}, \quad (2)$$

where  $i = \sqrt{-1}$ ,  $0 \leq k \leq N-1$ . In the Apollo data reduction programs,  $N$  was either 1024 or 2048 (see Table II). Each set of coefficients corresponds to a time interval  $T = N \cdot (\text{sampling interval})$  (see Table II for values). The outputs of the transformation are the  $f_k^n$  above.

Subtask 4

Generation of Coherency Matrix

The coherency matrix (Born and Wolf, 1959) was determined directly from the  $f_k^n$  by forming the summed products

$$\begin{bmatrix} \sum_{n=1}^L |f_k^n|^2 & \sum_{n=1}^L f_k^n f_k^{n*} \\ \sum_{n=1}^L f_k^{n*} f_k^n & \sum_{n=1}^L |f_k^n|^2 \end{bmatrix} \quad (3)$$

where \* denotes complex conjugate. Each sum is a function of the frequency index k. In order to compensate for the non-uniform effects of the receiving system filters, we further form

$${}_1\hat{q}_k^2 = \langle {}_1q_k^2 \rangle = \sum_{n=1}^M |{}_1q_k^n|^2 \quad (4)$$

$${}_2\hat{q}_k^2 = \langle {}_2q_k^2 \rangle = \sum_{n=1}^M |{}_2q_k^n|^2$$

where  $q_k^n = f_k^n$  for periods with signal absent. The  $\hat{q}_k^2$  are the receiving system output power spectra for a noise input. The upper bound M was chosen to reduce the fluctuations in  $\hat{q}_k^2$  to a small value. Typically  $M \lesssim 10^4$ , for which  $\hat{q}_k^2$  is determined to approximately one percent. The coherency matrix, corrected for receiver power transfer characteristics is

$$\underline{J}_k = \begin{bmatrix} J_{11} & J_{12} \\ J_{21} & J_{22} \end{bmatrix}, \quad (5)$$

Subtask 4 (cont.)

where

$$\begin{aligned}
 J_{11} &= \frac{1}{\hat{q}_k} \sum_{n=1}^L |f_k^n|^2 \\
 J_{22} &= \frac{1}{\hat{q}_k} \sum_{n=1}^L |f_k^n|^2 \\
 J_{12} &= \frac{1}{\hat{q}_k} \sum_{n=1}^L f_k^n f_k^{n*} \\
 J_{21} &= J_{12}^* .
 \end{aligned} \tag{6}$$

The fractional polarization of the received signal may be computed directly from the  $\underline{J}_k$  as

$$\gamma_k = \left\{ 1 - \frac{4 \text{ Det } \underline{J}_k}{\text{Trace}^2 \underline{J}_k} \right\}^{1/2} \tag{7}$$

Again  $\gamma_k$  is a function of the frequency index  $k$ . The output of Subtask 4 consists of the spectra  $\underline{J}_k$ ,  $\gamma_k$ . The parameters  $L$  and  $N$  used in the reduction of the several sets of observations are included in Table II. Completion of the  $\underline{J}_k$  (Subtasks 2, 3, and 4) represented the greatest portion of the computational expense for this experiment. Additional results may be obtained directly from  $\underline{J}_k$  and  $\gamma_k$ . For example, the power in the polarized and unpolarized parts of the echo is:

Subtask 4 (cont.)

polarized power  $P_p(k) = \gamma_k \cdot \text{Trace } \underline{J}_{-k}$  (8)

unpolarized power  $P_u(k) = (1-\gamma_k) \cdot \text{Trace } \underline{J}_{-k}$

Other parameters of the echo spectra may be obtained similarly (Born and Wolf, 1959; Appendix 10).

## Subtask 5

### Correction for System Polarization Parameters

The quantities  $\underline{J}_k$  and  $\underline{V}_k$  discussed in the previous section under Subtask 4 were derived directly from the sample data as they came from the analog tapes. As discussed under Subtask 4 certain corrections have been made for the receiver filter characteristics. However, the data were treated as though they were derived from perfect antennas. That is, the antennas were assumed to consist of a pair of right and left circularly polarized elements. It was further assumed that, with the exception of the filter corrections already applied, the gains in the two receiver channels were equal. In the case of the 13 centimeter data this assumption was very good. The isolation of the DSN 64 m antenna has been measured as  $> 26$  db with an axial ratio of  $\lesssim 0.8$  db (private communication, D. Bathker, JPL, 1973). At 116 cm the properties of the SRI 46 m antenna are not nearly so well known. Polarization of the 46 m antenna was controlled principally through the constraints applied to the construction of the feed system. The feed system consisted of a crossed dipole array of linear elements connected through a standard hybrid to obtain a circular polarization. The array elements were mechanically and electrically identical. The hybrid combiner and associated phase shift elements were adjusted to within  $1^\circ$  and 1 db of the ideal transfer function for such a device. Coupling between the orthogonal linear array elements was less than 40 db with the feed removed from the dish. Cross-coupling between the two circular polarizations, observed at the hybrid output with the feed in place at the focus of the dish, was 16 db. We were unable to measure the axial ratio of the overall system with the feed in place in the dish. We estimate axial ratio of the 116 cm system as approximately 1 db for either polarization. For certain received polarizations axial ratios

Subtask 5 (cont.)

of this magnitude can introduce significant errors in the calculation of fractional polarization. Consequently, a correction for this uncertainty was applied in Subtask 5. This correction was applied to the 116 cm Apollo 14 and 16 data only. The output tapes from Subtask 5 preserve the original  $\underline{J}_k$  computed earlier.

The corrections were determined as follows (cf Tyler, 1970). Consider the signals arriving at the antenna terminals in terms of their right and left circularly polarized components, which we will denote  $E_r$ ,  $E_l$ , respectively. The relationship between the arriving signals and the signals at the antenna terminals may be expressed as a matrix multiplication

$$\begin{bmatrix} E_r \\ E_l \end{bmatrix} = \begin{bmatrix} c_{11} & c_{12} \\ c_{21} & c_{22} \end{bmatrix} \begin{bmatrix} E_r \\ E_l \end{bmatrix} \quad (9)$$

where the  $c$ 's are complex and arbitrary. The matrix elements may be thought of as the transmission coefficients of the four port network consisting of pairs of antenna elements and terminals. Physically, the  $c$ 's may represent attenuation, gain, and cross-coupling. In an ideal system  $c_{11} = 1$ ,  $c_{12} = c_{21} = 0$ ,  $c_{22} = 1$ .

Subtask 4 (cont.)

The effect of such a transformation on the coherency matrix  $\underline{J}$  is easily shown to be

$$\begin{bmatrix} J'_{11} \\ J'_{12} \\ J'_{21} \\ J'_{22} \end{bmatrix} = \begin{bmatrix} |c_{11}|^2 & c_{11}c_{12}^* & c_{11}^*c_{12} & |c_{12}|^2 \\ c_{11}c_{21}^* & c_{11}c_{22}^* & c_{12}c_{21}^* & c_{22}^*c_{12} \\ c_{11}^*c_{21} & c_{21}c_{12}^* & c_{22}c_{11}^* & c_{22}c_{12}^* \\ |c_{21}|^2 & c_{22}^*c_{21} & c_{22}c_{21}^* & |c_{22}|^2 \end{bmatrix} \begin{bmatrix} J_{11} \\ J_{12} \\ J_{21} \\ J_{22} \end{bmatrix} \quad (10)$$

where  $\underline{J}'$  is the coherency matrix of the wave associated with  $\underline{J}$  observed at the antenna terminals. The  $k$  subscripts have been suppressed for convenience. However, it is assumed that the  $c$ 's are independent of frequency over the spectrum of interest. Given  $\underline{J}'$  and the  $c$ 's, the original  $\underline{J}$  may be recovered through an inverse matrix manipulation. In the present case  $\underline{J}'$  is observed, but the  $c$ 's are unknown.

The  $c$ 's may be estimated from an observation of an unpolarized signal (Tyler, 1970). System noise inputs to the 116 cm receiver system were used to estimate the  $c$ 's and perform a correction. The method was based on an experimenter selection of those portions of the receiver output spectrum that contained only receiver noise. If it is assumed that the noise input is unpolarized, then

$$\begin{aligned} J'_{11} &= (|c_{11}|^2 + |c_{12}|^2) J_0 \\ J'_{12} &= (c_{11}c_{21}^* + c_{22}^*c_{12}) J_0 \\ J'_{21} &= J_{12}^* \\ J'_{22} &= (|c_{21}|^2 + |c_{22}|^2) J_0, \end{aligned} \quad (11)$$

Subtask 5 (cont.)

where

$$\begin{aligned} J_0 &= k T_{\text{sys}}/2 \\ k &= 1.38 \times 10^{-23} \text{ (Joules/deg. Kelvin)} \\ T_{\text{sys}} &= \text{system temperature.} \end{aligned} \quad (12)$$

The signal will appear unpolarized if

$$J_{12}' = 0 \text{ and } J_{11}' = J_{22}'$$

or

$$c_{11}c_{21}^* = -c_{22}^*c_{12} \quad (13)$$

and

$$|c_{11}|^2 + |c_{12}|^2 = |c_{21}|^2 + |c_{22}|^2,$$

from which the required inverse transformation can be obtained. In practice, a numerical estimate of the correction matrix was obtained as described above. This estimate was then used as a starting point in a search to find the  $c$ 's which minimized the apparent polarization of the corrected  $J_{-k}'$  in the noise portions of the spectrum. The corrections in the form just described were then used to compute the corrected  $J_{-k}'$  for the entire spectrum. A corrected fractional polarization  $\gamma_k'$  based on  $J_{-k}'$  was then obtained.

The output tapes from Subtask 5 contain the original  $J_{-k}$  and the new, corrected  $\gamma_k'$ . A data user may easily recompute the original  $\gamma_k$  from the  $J_{-k}$  which have been preserved and which are available on the tapes supplied (see Subtask 6, Appendix IV). The correction factors employed in the generation of the  $\gamma_k'$  are given in Appendix VIII.

### Subtask 5 (cont.)

In summary, steps in this subtask are:

- a) Read  $\underline{J}_k$  source tapes from Subtask 4
- b) Determine elements of the correction matrix based on minimization of the polarized part of the noise.
- c) Compute  $\gamma_k'$ .
- d) Generate new tape containing the original  $\underline{J}_k$  and new  $\gamma_k'$ .

This process was applied to the Apollo 14 and 16 116 cm data: 13 cm data are uncorrected, i.e., for 13 cm data  $\gamma_k' = \gamma_k$ . In subsequent steps the  $\gamma_k'$  were used in all computations of the polarized and unpolarized parts of the 116 cm echo spectrum.

## Subtask 6

### Merging Observations with Trajectory

The output of Subtask 5, the  $\underline{J}_k, \gamma_k$  tapes, represents the experimenter's best estimate of the received spectra, averaged over the time intervals previously defined: that is, a complete second order description of the received echo signal. In the present step this data, which was previously processed without regard to lunar coordinates or other geophysical considerations, was combined with the Apollo command-service-module ephemeris. The ephemeris was first interpolated to the mid-point of the averaging period used in the computation of the  $\underline{J}_k$ , then certain ancillary quantities were computed. The interpolated ephemeris and the derived quantities were then merged with the experimental data to form a basic set of source tapes designated JM Doptrack. After further processing in Subtask 10, these tapes became the primary source tapes supplied with this report to the NSSDC.

The ephemeris based quantities added to the observational data were:

- a) Time corresponding to mid-point of averaging period
- b) Predicted difference between reflected and direct doppler shifts
- c) Predicted echo bandwidth for a moon with rms slope of 0.1
- d) Angle of incidence on mean spherical moon
- e) Spacecraft altitude above mean spherical surface
- f) Speed of the spacecraft
- g) Bistatic-radar cross-section of a smooth, perfectly conducting, spherical moon for the current spacecraft-moon-earth geometry
- h) Normalized signal strength for a conducting moon and instantaneous geometry
- i) Spacecraft position in selenographic coordinates
- j) Specular point position on a mean spherical lunar surface in selenographic coordinates

Subtask 6 (cont.)

- k) Selenographic latitude and longitude of spacecraft position
- l) Doppler shift due to rotation of the earth
- m) Total doppler shift of the reflected signal
- n) Selenographic latitude and longitude of specular point on the mean spherical lunar surface
- o) Speed of the specular point on the mean lunar surface
- p) Look angles to earth in spacecraft coordinates
- q) Euler angles of spacecraft attitude in local horizon system
- r) Selenographic unit velocity vector of spacecraft
- s) Selenographic unit vector location of earth.

These tapes are organized in groups of six data records, referred to as a data frame, corresponding to each time interval. A complete description of the JM Doptrack tape formats and contents is given in the appendixes (see Appendix IV).

## Subtask 7

### Computation of Polarized and Unpolarized Parts, Carrier Suppression

JM Doptrack tapes contain spectrally analyzed 13 cm and 116 cm receiver outputs. No provision was made within the receivers or Subtasks 2, 3, 4, 5, or 6 for removal of the directly propagating telemetry carrier from the echo data. In terms of the polarization parameters, this signal cannot be removed completely. However, much of the data analysis is based only on the low order moments of the polarized part of the echo. Subtask 7 computed polarized and unpolarized spectra from relation (8), Subtask 4, then used an empirically derived algorithm to remove the carrier signal from the polarized spectra; these data together with the ephemeris data described in Subtask 6 constitute the intermediate data set generated by Subtask 7. The algorithm for carrier suppression is described in Appendix V. Carrier suppression was also applied to unpolarized data. However, the carrier was largely suppressed in those data by coherency matrix processing, since it was a polarized signal. The output of this subtask, the P tapes, contain the experimenter's best estimate of the power spectra of the polarized and unpolarized components of the echo signal.

## Subtask 8

### Computation of Total Received Power, Echo Moments

Inputs to this subtask were the polarized and unpolarized power spectra derived from the JM Doptrack source tapes (Subtasks 6, 7). The purpose of Subtask 8 was to derive numerical measures of the echo spectra. Certain measures of the echo spectra were corrected for predictable trajectory effects and converted into scientific units. In all cases, the designation of the echo signal location in a spectrum was made by the experimenter's visually scanning plots of the polarized and unpolarized power spectra. The values of the  $k$  indices bounding the echo were input to a computer program that did the actual data reduction. An average noise level, determined from a region of the spectra not containing echo, was also input to the computer program. The data were monitored at approximately 30 sec. intervals and the echo limits reset to account for motion of the echo in the receiver passband. It was also necessary to occasionally reset the noise level as it also varied during the experiment, principally due to the scan of the receiving antenna across the lunar terminator. The derived quantities are given below:

- a) Polarized echo power -- the integral of the polarized power spectra between the frequency limits set by the experimenter and above the system noise level. This quantity is the best measure of the polarized echo power received.
- b) Normalized polarized echo power -- the quantity described in a) above, divided by the polarized system noise level.
- c) Unpolarized echo power -- the integral of the unpolarized power spectra between the frequency limits set by the experimenter and above the system noise level. This quantity is the best measure of the unpolarized echo power received.
- d) Normalized unpolarized echo power -- the quantity described in c) above, divided by the unpolarized system noise level.

Subtask 8 (cont.)

- e) Equivalent area bandwidth -- the bandwidth of the polarized echo signal between the frequency limits set by the experimenter and above the polarized system noise level as determined by the ratio of the total polarized echo power to the peak polarized echo power.
- f) Normalized absolute moment bandwidth -- the bandwidth of the polarized power echo as described in e) above, computed from a gaussian equivalent absolute moment, and divided by e).
- g) Normalized second moment bandwidth -- the bandwidth of the polarized power echo as described in e) above, computed from a gaussian equivalent second moment, and divided by e).
- h) Centroid of echo spectrum -- the centroid of the polarized power echo as described in e) above.
- i) RMS slope -- the rms slope of the lunar surface inferred from the value of e) above and the predicted bandwidth for an rms surface slope of 0.1, using linear interpolation.

Formulas for the computation of the above quantities and a brief explanation of their use may be found in Appendix VI. The trajectory data added in Subtask 6 were retained throughout this subtask. A simple correspondence between the output of this subtask and the JM Doptrack tapes was maintained through inclusion of ephemeris data in both data sets.

## Subtask 9

### Final Editing of Data

Final editing of the output from Subtask 8 resulted in a set of reduced data records designated Integral tapes. These tapes constitute the second form of data supplied to the NSSDC.

Final editing of data included the following steps:

- a) Addition of hand-scaled bandwidths as a partial independent check on Subtask 8 (see Subtask 10).
- b) Addition of spacecraft antenna gain in the direction of specular reflection.
- c) Notation of operational or data processing changes
  - i) Polarized band bad
  - ii) Unpolarized data bad
  - iii) Change in polarized noise level
  - iv) Change in polarized k indices for echo limits
  - v) Change in unpolarized noise level
  - vi) Change in unpolarized k indices for echo limits
  - vii) Change in system gain

Caution: Some integral data, primarily at the beginning or end of a transmission, have been deleted. Large overlaps in the 13 cm data caused by the use of two analog tape recorders have also been deleted. In all other cases bad data, for example when interference is present, are flagged on the edited Integral tapes as described in c) above (see Appendix VI, E47). The data contained on the Integral tapes are still the experimenter's best estimates of the values. However, in the case of flagged data, that estimate may be very poor. No flagged data should be used without examining the spectra on the corresponding JM Dop-track tapes. For example, in the 116 cm data occasional interference produced marked increases in the apparent polarized echo power, but evidently left the unpolarized

Subtask 9 (cont.)

power unaffected. A flag for polarized power thus may also cast suspicion on the unpolarized power. The experimenters have evaluated these cases and indicated their opinions accordingly in the data. Other individuals may arrive at different conclusions. It is primarily for this reason that the JM Doptrack/Integral tape frame-to-record correspondence (through ephemeris data) has been maintained: reduced data records on the Integral tapes may, if questioned, be re-evaluated from the JM Doptrack source tapes. A complete description of the Integral tape formats and the flags is given in Appendix VI.

## Subtask 10

### Displaying, Scaling, and Copying the Data

Output from Subtask 6, the JM Doptrack tapes, is used in miscellaneous programs in preparation for data analysis and distribution. An important step in producing the final Integral tapes (Subtask 9) took place here. Polarized power spectra obtained from JM Doptrack tapes are computer plotted and visually examined to determine specifically

- a) proper receiver operation
- b) proper receiver tuning
- c) presence of interference.

Such plots are also used to determine the one-half power, hand-scaled bandwidths added to the data set in Subtask 9. This bandwidth is determined by measuring the width of the polarized echo spectrum at a point one-half the distance from the apparent system noise level to the mean echo peak. The measured distance is scaled by the appropriate factor to determine the width in Hertz. Such measures can be related to the rms slope of the lunar surface from the quasi-specular scattering theory (see Appendix VI). The hand-scaled values are used to verify the machine algorithms used in computing lunar rms slopes and as a simple means of quickly estimating the slope.

Finally, this subtask included copying of the JM Doptrack tapes for shipment to the NSSDC. These tapes were not edited.

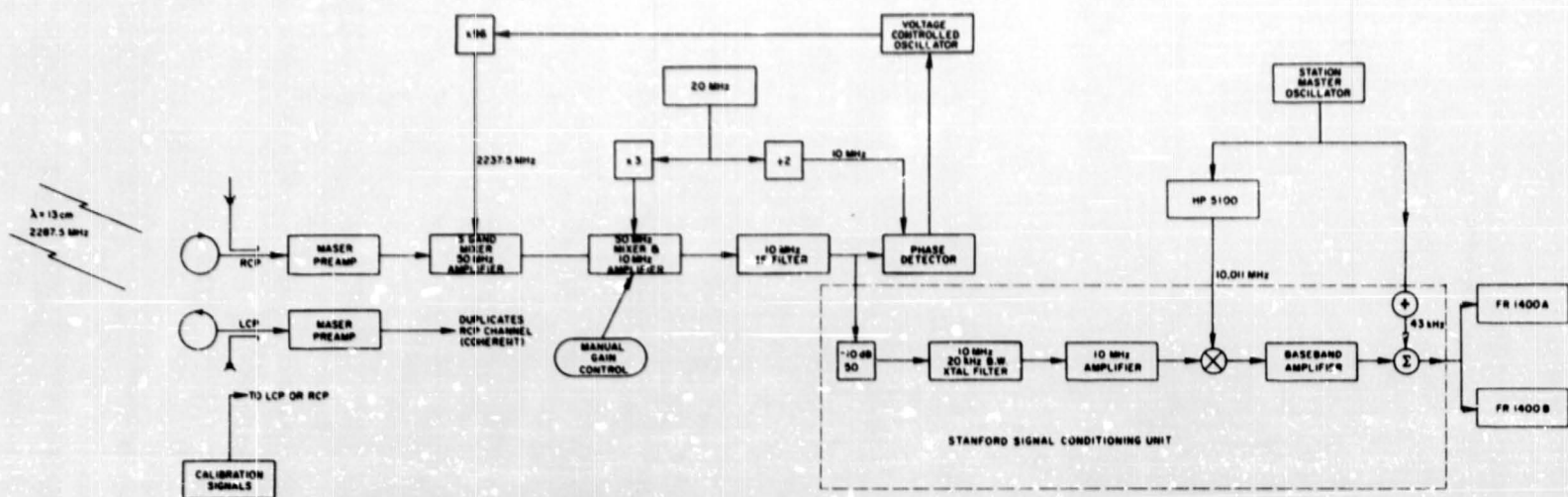
## Subtask 11

### Utility Routines

Integral tapes have been organized as a sequence of records describing the data and experimental geometry at successive instances of time. It is then a simple matter to determine any set of variables from this tape with time as a parameter. We suggest that data users consider this data as a set of dependent functions parameterized in time and hope that such a presentation is found useful.

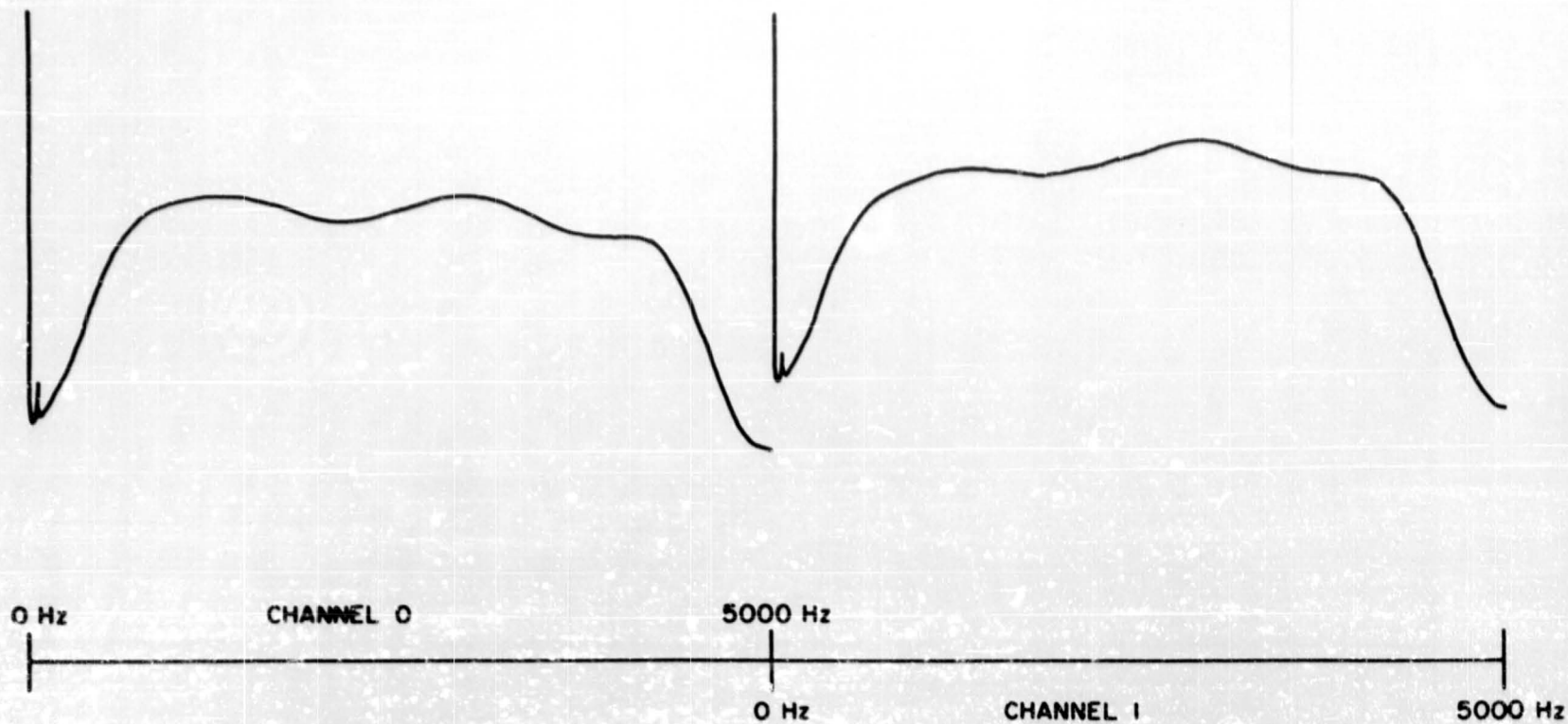


## APPENDIX II



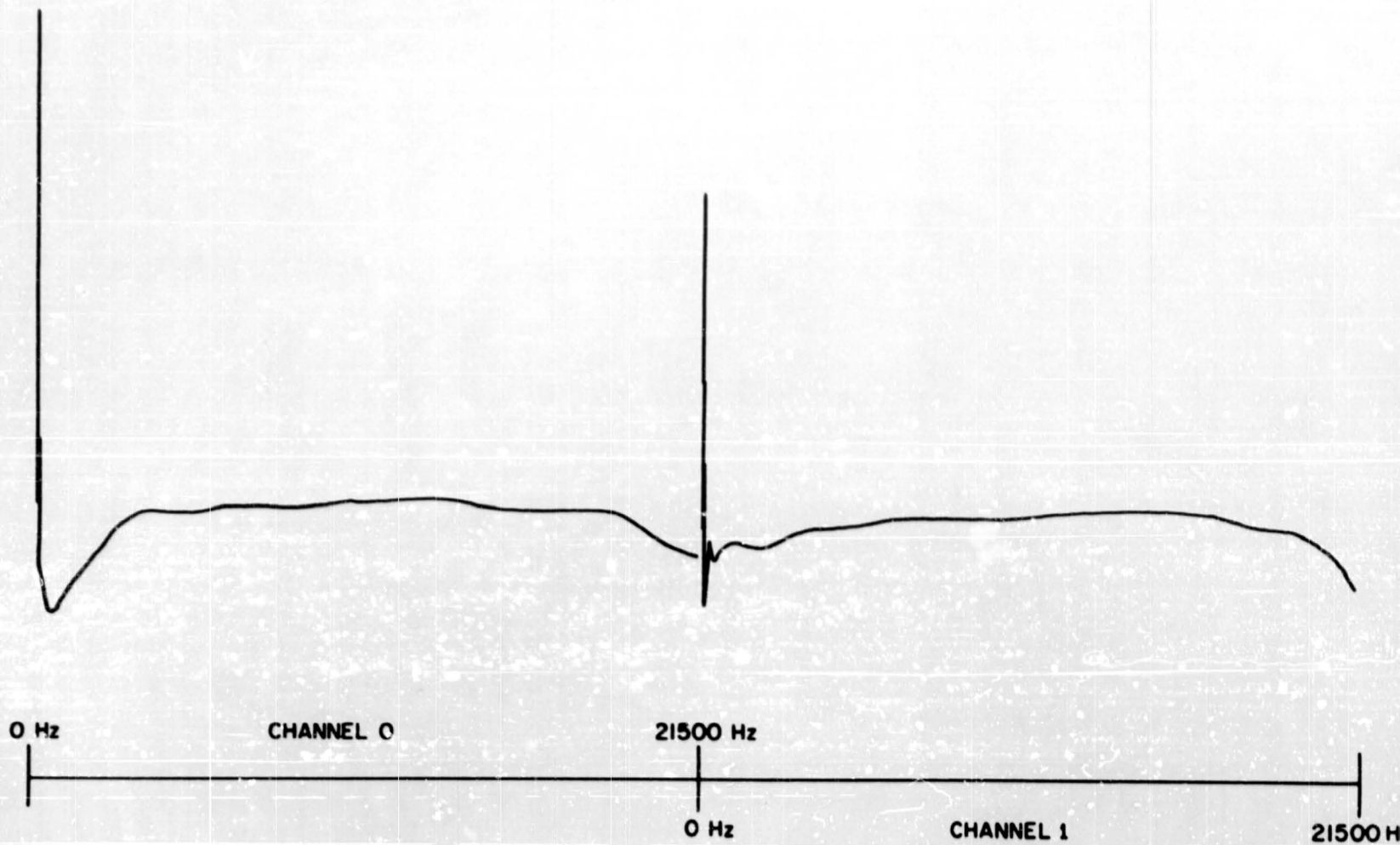
Stanford Apello 13 cm (S-Band) Bistatic-Radar Receiving System:  
Major Elements

APPENDIX III



Apollo Bistatic-Radar Receiving System  
116 cm Uncorrected Frequency Response

APPENDIX III (cont.)



Apollo Bistatic-Radar Receiving System  
13 cm Uncorrected Frequency Response

## Appendix IV

### JM Doptrack Tape Formats

This appendix describes the tape formats for the JM Doptrack Tapes generated in Subtask 6 of the text. Tapes are 9 track, binary in XDS Sigma 5 machine images.<sup>o</sup> These tapes contain the output of the polarimeter in Subtask 4, the corrected fractional polarization obtained from Subtask 5, MSC trajectory data, and certain ancillary quantities computed at Stanford. All records within the given file are the same length. There may be more than one tape per file. Files are identified by a header record which contains a brief description of the file contents. This appendix describes the tape organization, the file organization, and the record formats for the JM Doptrack tapes. Definitions of the tape contents are either given here or described by reference.

#### A. File Organization

File	No. Tapes	Contents	Record Length
1	1	Apollo-14 116 cm	514 words
2	1	Apollo-14 13 cm	514 words
3	1	Apollo-15 116 cm	1026 words
4	2	Apollo-15 13 cm	514 words
5	1	Apollo-16 116 cm	1026 words
6	2	Apollo-16 13 cm	514 words

#### B. File Organization

##### 1. Header Record

2. Data Record	1	} Observational Data	} Data Frame
Data Record	2		
Data Record	3		
Data Record	4		
Data Record	5		
Data Record	6	Ephemeris Data	

⋮  
 < Many Data Frames >  
 ⋮

##### 3. EOF (End of File Mark)

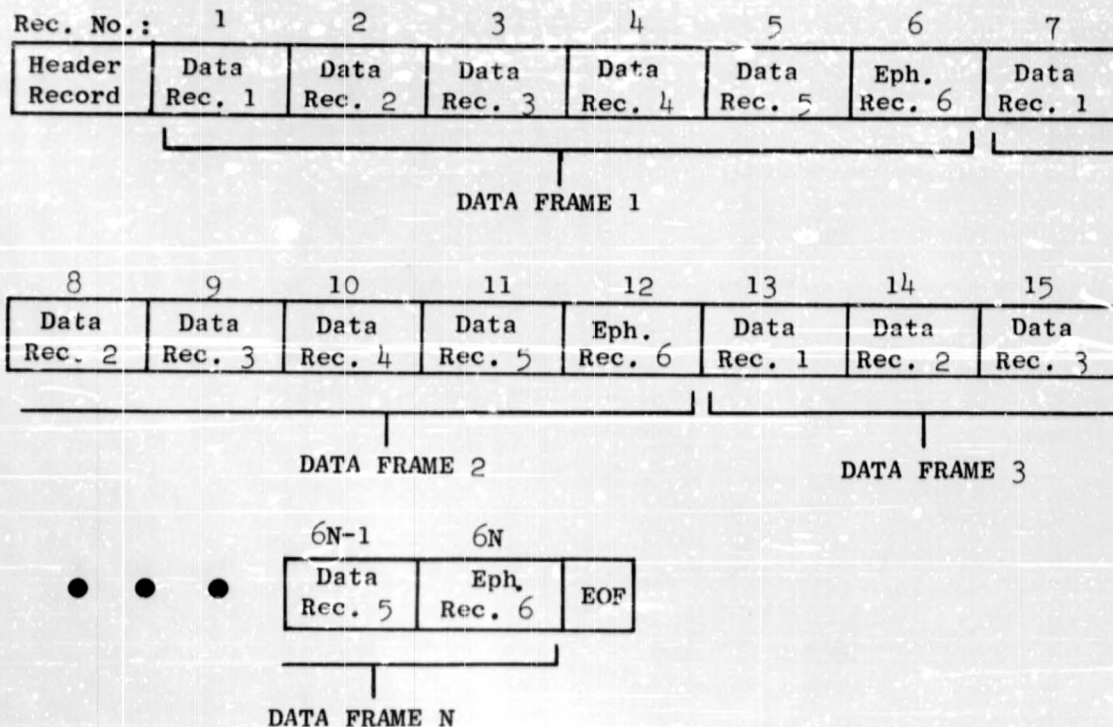
<sup>o</sup>See Appendix XI for a description of Sigma 5 machine images.

Appendix IV (cont.)

If more than one tape was needed to contain the JM Doptrack file, the file was continued across the end of the tape to the next tape without interruption; there is only one header record per file, at the beginning of the first tape of the file.

Once again, even though the files are physically nothing more than a continuous string of records, all of equal length, it is helpful to think of them (see figure below) as being composed of a header record followed by groups (frames) of six records. The ephemeris data record concludes the frame and, since each JM data frame is a short-time average, the ephemeris data have been calculated using the midpoint of the frame as the instantaneous time reference point.

JM Doptrack File Containing N Data Frames



Appendix IV (cont.)

C. Header Record Formats

<u>Word No.</u>	<u>Contents</u>	<u>Units</u>	<u>Machine Type</u> <sup>α</sup>
1-42	Alphanumeric file identifier	--	A
43	Day of year on which data were collected (January 1 = 1)	(days)	I
44	Year data were taken (Gregorian)	(year)	I
45-46	Julian Ephemeris Day at 00:00 UT2 on the day the data were taken	(days)	DPR
47-48	Julian Ephemeris Day of reference epoch	(days)	DPR
49	Time increment between centerpoint of data averaging frame	(sec)	R
50	Number of data records following this header record (Number of data frames = number of data records divided by 6)	--	I
51-514/1026	Not used		

D. Data Frame Formats

1. Data Record Organization

<u>Record No.</u>	<u>Contents</u>	<u>Note:</u>
1	$J_{11}(k)$	116 cm data $J_{11}(k)$ - Left circular polarization
2	$J_{22}(k)$	
3	Real part of $J_{12}(k)$	$J_{22}(k)$ - Right circular polarization
4	Imaginary part of $J_{12}(k)$	
5	$\gamma(k)$	
6	Spacecraft ephemeris and ancillary data	13 cm data $J_{11}(k)$ - Right circular polarization
		$J_{22}(k)$ - Left circular polarization

<sup>α</sup>A - Alphanumeric

I - Integer

R - Real

DPR - Double Precision Real

Appendix IV (cont.)

D. 2. Format Records 1-5 (all machine type real)<sup>ω</sup>

<u>Record No.</u>	<u>Contents</u>
1-513/1025	Data described under D.1 above
514/1026	Meaningless

3. Format Record 6 (all machine type real)

<u>Word No.</u>	<u>Contents</u>	<u>Units</u>
1	Meaningless	
2	UT2 at midpoint of frame	(sec)
3	Reflected doppler minus direct doppler	(Hz)
4	Predicted bandwidth for rms surface slope of 0.1	(Hz)
5	Angle of incidence	(deg)
6	Spacecraft altitude (mean lunar radius assumed 1736 km)	(km)
7	Spacecraft speed	(m/sec)
8	Radar cross section predicted for smooth conducting moon	(dim)
9	(Radar cross section)/ (received power)	(m <sup>2</sup> /w)
10	X } Components of selenographic unit position Y } vector of spacecraft Z } location	(dim)
11		
12		
13	X } Components of selenographic unit position Y } vector of specular Z } point location	(dim)
14		
15		
16	Selenographic latitude of subspacecraft position	(deg)
17	Selenographic longitude of subspacecraft position	(deg)
18	Component of doppler shift due to earth rotation	(Hz)

<sup>ω</sup>Due to a hardware problem in the data processing, words 1-15 are zero in the Apollo-14, 116 and 13 cm, and Apollo-15 13 cm files.

Appendix IV (cont.)

D. 3. Format Record 6 (all machine type real) (cont.)

<u>Word No.</u>	<u>Contents</u>	<u>Units</u>
19	Total doppler shift of reflected signal	(Hz)
20	Selenographic latitude of specular point	(deg)
21	Selenographic longitude of specular point	(deg)
22	Speed of specular point on the lunar surface	(M/sec)
23	$\alpha_e$ } Vehicle look angles $\beta_e$ } to earth	
24		
25	$\theta$ } Euler angles of local $\psi$ } horizon coordinates $\phi$ }	(deg)
26		
27		
28	$X$ } Spacecraft selenographic $Y$ } unit velocity vector $Z$ }	(dim)
29		
30		
31	$X$ } Selenographic unit $Y$ } vector from center of $Z$ } moon to center of earth	(dim)
32		
33		
34-514/1026	Not used	

**Note:** Data do not always progress uniformly in time. Occasionally, data frames will reverse in time for one frame, and then continue forward. This effect is caused by the sampling procedure in which deliberate overlap was inserted. Time on data is correct.

E. Definition of Contents

1. Data -- defined under Subtasks 4 and 5 of the text.
2. Ephemeris and Ancillary Data -- described in greater detail in Appendix VI.

## Appendix V

### Carrier Suppression Algorithm

This appendix describes the algorithm used to remove the direct signal from the polarized and unpolarized parts of the bistatic-radar echo spectrum (see Subtask 7). This algorithm was used on each frame of polarized and unpolarized data which the JM Doptrack tapes yield according to relation (8), Subtask 4. Two slightly different procedures were used for the 116 cm and 13 cm data. These differences constituted the only difference in procedure between the 116 cm and 13 cm data. Both data sets were processed by the same computer program, with different program branches for the two cores. The direct signal observed at 13 cm was free of spurious sidebands to the level of our observations. At 116 cm, the direct signal contained two weak sidebands symmetrically displaced approximately 20 db below the direct signal. Consequently, during periods of strong direct signal at the 116 cm wavelength, it was also necessary to correct for the presence of these sidebands. The procedures described below were developed empirically but were found to give good results. The approach was to find the maximum of the power spectrum and to assume that this maximum represented the direct signal. This assumption was tested by determining the height of the maximum with respect to the fluctuations in the spectrum in the immediate vicinity of the maximum. If the maximum exceeded the fluctuation criteria then an interpolation procedure was used to provide a smoothed estimate of the spectrum. In the case of the 116 cm data, sideband suppression was achieved by reducing the local maximum on either side of the direct signal by an amount proportional to the strength of the direct signal. A detailed summary of this procedure is given below.

#### Initial Test

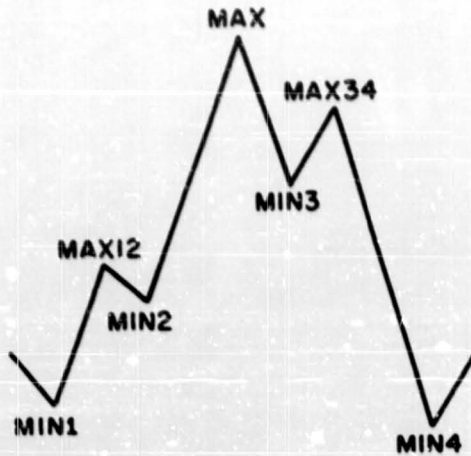
1. Find the absolute maximum of all the data, MAX (see figure which follows).
2. Find the adjacent local maxima, MAX<sub>12</sub> and MAX<sub>34</sub>.
3. Test MAX to determine whether or not it represents the direct signal.

$$i) \quad \text{SUM} = \frac{\text{MIN}_1 + \text{MIN}_2}{8} + \frac{\text{MAX}_{12}}{4} + \frac{\text{MIN}_3 + \text{MIN}_4}{8} + \frac{\text{MAX}_{34}}{4}$$

Appendix V (cont.)

Initial Test (cont.)

- ii)  $CRIT = 1.2 \cdot SUM$
  - iii) (MAX.LT.CRIT)  $\Rightarrow$  no direct signal present, terminate procedure; go to next frame, initial test 1.  
(MAX.GE.CRIT)  $\Rightarrow$  direct signal present, continue.
4. Check data type. If data is 116 cm then go to step 8, otherwise continue with step 5.



13 cm Procedure

5. Test for a smooth direct signal.

IF  $(2.0 \cdot MIN1.GE.MIN2)$   
and  $\Rightarrow$  smooth direct signal.  
 $(2.0 \cdot MIN4.GE.MIN3)$

If the direct signal is smooth then all values between MIN2 and and MIN3 which are greater than CRITC are set equal to CRITC and the procedure is terminated; initial test 1 is then begun on the next frame. If the test for smoothness is failed, then continue with step 6.

6. This procedure is applied only if the direct signal is spread through several frequency analysis bins. Determine the first minimum on either side of the direct signal which

Appendix V (cont.)

Initial Test (cont.)

satisfies the following condition:

$(\text{MIN}(\hat{I}) . \text{LT} . \text{MIN}(\hat{I}-1) \cdot 2.0)$  Where  $\hat{I}$  indexes the left side of the direct signal

$(\text{MIN}(\hat{J}) . \text{LT} . \text{MIN}(\hat{J}+1) \cdot 2.0)$  and  $\hat{J}$  indexes the right side of the direct signal (see fig. below).

If the conditions are not satisfied in 15 minima, choose the 15th minima. Denote the extreme minima  $\hat{I}$ ,  $\hat{J}$ .  $\text{MIN}(\hat{I})$  and  $\text{MIN}(\hat{J})$  locate the extent of the spread direct signal.

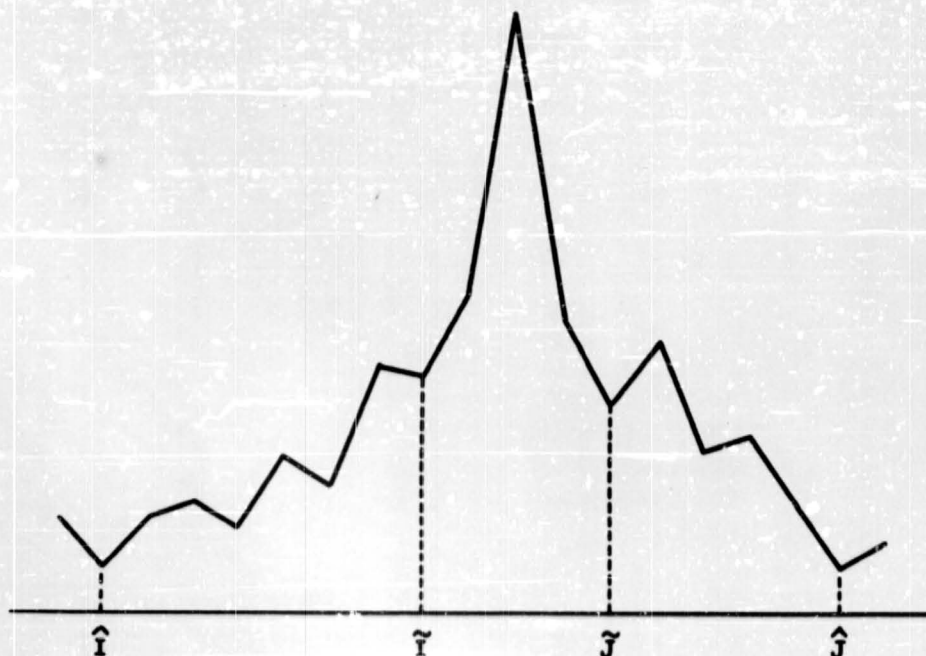
Denote the minima adjacent to the direct signal  $\tilde{I}$ ,  $\tilde{J}$ . Then replace the data  $D(\ )$  with  $D'(\ )$  calculated as follows:

$$D'(L) = D(L) - \frac{D(\tilde{I}) - D(\hat{I})}{\tilde{I} - \hat{I}} \cdot (L - \hat{I}); \quad \hat{I} + 1 \leq L \leq \tilde{I} - 1$$

$$D'(L) = D(L) - \frac{D(\hat{J}) - D(\tilde{J})}{\hat{J} - \tilde{J}} \cdot (L - \hat{J}); \quad \tilde{J} + 1 \leq L \leq \hat{J} - 1$$

$$D'(L) = D(\tilde{I}) + \frac{D(\tilde{J}) - D(\tilde{I})}{\tilde{J} - \tilde{I}} \cdot (L - \tilde{I}); \quad \tilde{I} \leq L \leq \tilde{J}$$

7. Terminate procedure; go to next frame, initial test 1.



Appendix V (cont.)

116 cm Procedure

8. Find the largest local maximum within 60 Hz of the direct signal on first the left side and then on the right side of the direct signal. Designate these maxima MAXL, MAXR, respectively.
9. Determine relative magnitude of the direct signal.

$$\text{CRITSB} = 200.0 \cdot \text{SUM}$$

If  $(\text{MAX.GE.CRITSB})$  then the direct signal is sufficiently large to require compensation for the sidebands. Replace MAXL and MAXR by the average value of their respective adjacent minima.

10. If  $(\text{MAX.LT.CRITSB})$  the direct signal is small. Subtract a constant from the maxima MAXL and MAXR, defined above. The constant is

$$\text{ESUB} = (\text{MAX} - \text{SUM})/500.0$$

The subtraction is performed only if the data value is greater than ESUB.

11. Replace MAX by the average of MIN2 and MIN3.
12. Terminate procedure and go to next frame, initial test 1.

## Appendix VI

### Integral Tape Format

The Integral tape contains reduced data records generated in Subtask 7, 8 and 9 (see Block Diagram I). This appendix gives the detailed formatting of that tape and describes all ancillary computations.

#### A. Tape Organization

The table below gives the file contents and data record length for the Integral tape.

<u>File No.</u>	<u>Contents</u>	<u>Record Length</u>
1	Apollo-14 116 cm	50 words
2	Apollo-14 13 cm	50 words
3	Apollo-15 116 cm	50 words
4	Apollo-15 13 cm	50 words
5	Apollo-16 116 cm	50 words
6	Apollo-16 13 cm	50 words

The tape is 9 track, 800 BPI, binary in XDS Sigma 5 machine images. See Appendix XI for a description of Sigma 5 machine images.

#### B. File Organization

1. Header Record
2. Data Record  
:  
:  
<many data records>  
:  
:
3. (EOF) End of File
4. Header Record
5. :  
:  
:

Appendix VI (cont.)

C. Header Record Format

<u>Word No.</u>	<u>Contents</u>	<u>Units</u>	<u>Machine Type</u> <sup>α</sup>
1-42	Alphanumeric file identifier	--	A
43	Day of year on which data were collected (January 1 = 1)	(days)	I
44	Year data were taken	(year)	I
45-46	Julian Ephemeris Day at 00:00 UT2 on the day the data were taken	(days)	DPR
47-48	Julian Ephemeris Day of reference epoch	(days)	DPR
49	Time increment between center-point of data averaging frame	(sec)	R
50	Number of data records following this header record	--	I

D. Data Record Format (all machine type real)

<u>Word No.</u>	<u>Contents</u>	<u>Units</u>	
1	Meaningless		
2	UT2 at midpoint of frame	(sec)	
3	X } Components of selenographic unit position vector of spacecraft location	(dim)	
4			Y }
5			Z }
6	X } Components of selenographic velocity unit vector	(dim)	
7			Y }
8			Z }
9	Speed: Magnitude of spacecraft velocity vector	(m/sec)	
10	X } Components of selenographic unit vector from center of the moon to center of the earth	(dim)	
11			Y }
12			Z }

<sup>α</sup>A - Alphanumeric  
 I - Integer  
 R - Real  
 DPR - Double Precision Real

Appendix VI (cont.)

D. Data Record Format (all machine type real) (cont.)

<u>Word No.</u>	<u>Contents</u>	<u>Units</u>
13	X } Components of selenographic unit position Y } vector of specular Z } point location	(dim)
14		
15		
16	θ } Euler angles of spacecraft attitude and ψ } local horizon frame φ }	(deg)
17		
18		
$\bar{A}_{veh} = \begin{bmatrix} \phi \\ (x) \end{bmatrix} \begin{bmatrix} \psi \\ (z) \end{bmatrix} \begin{bmatrix} \theta \\ (y) \end{bmatrix} \begin{bmatrix} \bar{A}_1 \end{bmatrix} \left( \begin{array}{l} \text{cw rotation look-} \\ \text{ing in + axis} \\ \text{direction} \end{array} \right)$		
19	α <sub>s</sub> } Vehicle look angles to specular β <sub>s</sub> } point	(deg)
20		
21	δ Angle between plane of incidence and plane containing both the vehicle x axis and direction vector to specular point	
22	α <sub>e</sub> } Vehicle look angles to earth β <sub>e</sub> }	(deg)
23		
24	Selenographic latitude of spacecraft position	(deg)
25	Selenographic longitude of spacecraft position	(deg)
26	Selenographic latitude of specular point	(deg)
27	Selenographic longitude of specular point	(deg)
28	Angle of incidence	(deg)
29	Instantaneous speed of specular point on lunar surface	(m/sec)
30	Predicted bandwidth for rms surface slope of 0.1	(Hz)
31	Reflected doppler minus direct doppler	(Hz)
32	Total doppler shift of reflected signal	(Hz)
33	Component of doppler shift due to earth rotation	(Hz)

Appendix VI (cont.)

D. Data Record Format (all machine type real) (cont.)

<u>Word No.</u>	<u>Contents</u>	<u>Units</u>
34	Altitude of spacecraft above lunar surface; Radius of the moon assumed to be 1736 Km	(Km)
35	Radar cross-section predicted for smooth conducting moon	(dim)
36	(Radar cross-section)/ (received power)	(m <sup>2</sup> /w)
37	Polarized power	(arb)
38	Normalized polarized power	(°k)
39	Unpolarized power	(arb)
40	Normalized unpolarized power	(°k)
41	Equivalent area bandwidth	(Hz)
42	Normalized absolute moment bandwidth	(dim)
43	Normalized second moment bandwidth	(dim)
44	Centroid of the echo spectrum	(Hz)
45	RMS slope inferred from equivalent area bandwidth	(deg)
46	Spare if value equals zero, otherwise handscaled one-half power echo bandwidth	(Hz)
47	Data validity flag	
48	Spare if value = 0, otherwise value of spacecraft antenna gain in $\alpha_s, \beta_s$ , direction (see word no. 19, 20)	(dim)
49	Not used	
50	Data record sequence number	

**Note:** Data do not always progress uniformly in time. Occasionally, data records will reverse in time for one record, and then continue forward. This effect is caused by the sampling procedure in which a small deliberate overlap was inserted. Time tags on data are correct. Overlapping data correspond to the same time interval but different sampling passes. Slight differences arise from variation in exact times averaged.

Appendix VI (cont.)

E. Data Parameter Definitions

The remainder of this section defines the contents of the data records described just above. The individual subsection numbers correspond to the word numbers in Section D (Data Record Format). If a particular quantity has been described at length elsewhere, a reference will be given. Otherwise, the quantity is defined here.

1. Meaningless
2. Time is the UT2 in seconds at which the data were taken. This time corresponds to the mid-point of the averaging interval, as described under Subtask 4. All trajectory parameters have been interpolated to this time, so that geometrical quantities correspond to the location of the specular point on the mean lunar surface at the middle of the averaging interval.
- 3, 4, 5. Selenographic Unit Position Vector is defined with respect to the lunar surface. This vector is a unit vector directed from the center of the moon for the instantaneous location of the spacecraft. The X, Y, Z directions are defined as follows:
  - X = mean earth direction
  - Y = mean direction of the following limb
  - Z = north polar direction.
- The selenographic coordinates were obtained by rotation from the selenocentric geo-equatorial units of the epoch given in the header record. Procedures are described elsewhere (Tyler, 1968).
- 6, 7, 8. Selenographic Unit Velocity Vector is a unit vector in the direction of the spacecraft velocity. The coordinate system is the same as that given in items 3, 4, 5 above.
9. Speed is the magnitude of the spacecraft velocity vector.
- 10, 11, 12. Selenographic Unit Vector to Earth is a unit vector giving the direction from the lunar center of mass to the center of mass to the earth in the selenographic coordinate system described in the 3, 4, 5 above.

Appendix VI (cont.)

- 13, 14, 15. Selenographic Unit Position Vector of Specular Point is a unit vector from the center of mass of the moon to the location of the specular point on the mean spherical lunar surface. For this computation the lunar radius was taken as 1736 km. The specular point is the location on the mean lunar surface where the angles of incidence and reflection are equal (cf Tyler, 1968).
- 16, 17, 18. Euler Angles of Spacecraft Attitude connect the spacecraft altitude with a local horizon reference frame. Both the Local Horizon system and the Euler angles are defined in Appendix IX.
- 19, 20. Look Angles to Specular Point are in vehicle polar coordinates. These quantities are defined in Appendix IX.
21. Plane of the Vehicle, the orientation with respect to the plane of incidence, is given by the angle  $\delta$ . This quantity is necessary to define the vehicle attitude with respect to the plane of incidence. The angle  $\delta$  is defined in Appendix IX.
- 22, 23. Look Angles to Earth are the vehicle polar coordinates of a unit vector in the earth center of mass direction. These quantities were computed in the same manner as items 19, 20 above using the unit vector to earth.
24. Selenographic Latitude of Spacecraft Position is the selenographic latitude of the subspacecraft point computed from the Z component of the unit vector given in items 3, 4, and 5.
25. Selenographic Longitude of Spacecraft Position is the selenographic longitude of the subspacecraft position computed from items 3, 4, and 5 according to astrometric convention, western limb of the moon leading.
26. Selenographic Latitude of Specular Point is the selenographic latitude of the specular point on a mean spherical lunar surface computed from item 15.
27. Selenographic Longitude of Specular Point is the selenographic longitude of the specular point on the mean spherical lunar surface computed from items 13, 14, 15.

Appendix VI (cont.)

28. Angle of Incidence is the angle of incidence on mean spherical lunar surface at the specular point (cf Tyler, 1968).
29. Speed of the Specular Point is the speed with which the instantaneous specular point moves across the mean lunar surface (Tyler, 1968).
30. Predicted Bandwidth is the one-half power spectral width predicted for an rms surface slope of 0.1, based on the instantaneous angle of incidence and specular point velocity. Computation is after Fjeldbo (1964), also described in Tyler, (1968). Fjeldbo gives a theoretical expression for the 1/2 power echo bandwidth:

$$\Delta f = 4(2 \ln 2)^{1/2} \frac{v_s}{\lambda} \frac{h_o}{d_o} \cos \phi ,$$

where  $v_s$  = velocity of the specular point on the mean lunar surface,  $\lambda$  = wavelength of the radiation (either 116 cm or 13 cm),  $\phi$  = angle of incidence at the specular point, and the quantity  $\frac{h_o}{d_o}$  = the mean lunar rms slope.

The quantity  $\Delta f$  is the 1/2 power bandwidth predicted for a gaussian spectrum. Such a spectrum would result from a gently undulating surface with gaussian autocorrelation function.

31. Difference Between Reflected and Direct Doppler Shifts is the predicted frequency difference between a wave reflected from the specular point and the signal traveling directly from the spacecraft to earth. Sign convention is such that the difference is positive for a reflected doppler shift greater than the direct doppler shift.
32. Doppler Shift is the total doppler shift expected from the reflected signal. Computation of this doppler shift included spacecraft motion and the earth's rotation, but did not include the rate of change of distance between the earth and the moon.
33. Doppler Due to Earth's Rotation is the component of the observed doppler shift due to the earth's rotation, for a signal arriving from the direction of the moon.

Appendix VI (cont.)

34. Altitude of the spacecraft above the lunar surface has been computed assuming a lunar radius equal to 1736 km. The magnitude of the spacecraft radius vector from the lunar center of mass is obtained by adding the contents of word no. 34 to 1736 km.

35. Normalized Bistatic-Radar Cross-Section is the bistatic-radar cross-section of a smooth conducting sphere of the same radius and relative geometry as the moon. Following Fjeldbo (1964) this cross-section is given by

$$\sigma_B = \frac{4\pi R_1^2 \cos \phi}{\left(\cos \phi + \frac{2d_{or}}{R}\right) \left(1 + \frac{2d_{or} \cos \phi}{R}\right)},$$

where

$R_1$  = distance from transmitter to the center of the moon

$R$  = lunar radius ( $1.736 \times 10^6$  m)

$\phi$  = angle of incidence (cf item 28)

$d_{or}$  = distance from the transmitter to the specular point on the mean lunar surface.

36. (Radar Cross Section)/(Received Power) is a multiplicative constant relating instantaneous geometry and received power to surface reflectivity.

$$\frac{\text{radar cross-section}}{\text{received power}} = \frac{(4\pi)^2 R_1^2 R_2^2}{A P_T G_T \sigma_B}$$

where

$R_1$  = distance from transmitter to center of the moon

$R_2$  = distance from receiving site to center of the moon

$A$  = effective aperture of receiving antenna

$P_T$  = transmitted power

$G_T$  = transmitting antenna gain in specular point direction

$\sigma_B$  = bistatic-radar cross-section for a perfectly conducting moon.

For convenience, this expression was evaluated with the following numerical values for the quantities above:

Appendix VI (cont.)

$R_1$  = instantaneous value from MSC trajectory

$\sigma_B$  = instantaneous value from item 35 above

$R_2 = 4 \times 10^8$  m

$A = 0.5 (22.5)^2 \pi$

$G_T = 1$

$P_T = 2.5$  w.

These values give only order of magnitude results for this experiment.

37. Polarized Power is the experimenter's best estimate of the polarized component of the received echo total power. Extraction of the polarized power is discussed elsewhere (cf Subtask 8).

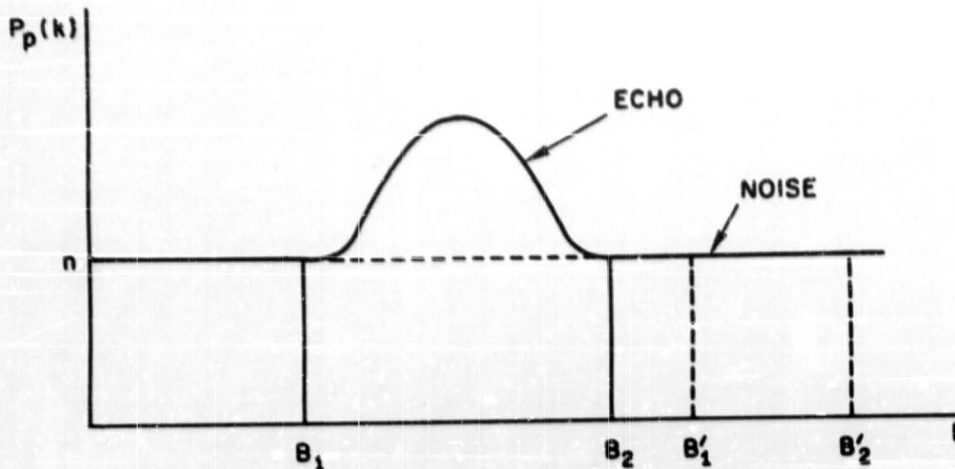
Denote the polarized power spectrum  $P_p(k)$ . Consider the figure below. Polarized power is determined from

$$P = \sum_{k=B_1}^{B_2} (P_p(k) - n).$$

The  $P_p(k)$  is a polarized power spectrum. In the determination of  $P$ , the signal limits  $B_1$ ,  $B_2$  and  $n$  were selected by the experimenter. The quantity  $n$  was chosen on the basis of

$$\sum_{k=B_1'}^{B_2'} (P_p(k) - \hat{n}) \sim 0$$

where  $B_1'$ ,  $B_2'$  represent spectral limits containing no echo signal, and  $\hat{n}$  represents a sequence of trials of  $n$ . The limits  $B_1$ ,  $B_2$ ,  $B_1'$ ,  $B_2'$ , were varied as is necessary to follow the changing echo signal.



38. Normalized Polarized Power is the quantity contained in item 37 divided by the average power spectral density of the system noise level. This quantity has been discussed in detail elsewhere (cf Subtask 8).

Using the notation introduced under item 37,

$$\text{normalized polarized power} = P/n,$$

where  $P$  and  $n$  have the same meaning as above.

Note:  $P/n$  is extremely sensitive to the choice of  $n$ . Thus, polarized power is considered the best overall measure of received polarized echo power. But  $P/n$  provides the only method, through the measure of system temperature, of obtaining an absolute power calibration. Similarly, the value of  $n$  may be determined from the ratio of polarized power to  $P/n$ , so that the variations and system temperature and/or gain may be estimated.

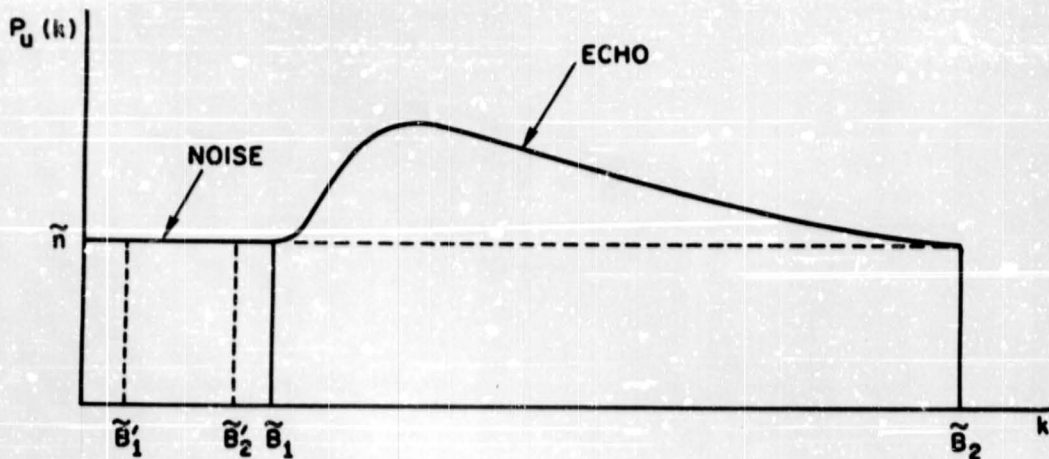
39. Unpolarized Power is the analogous quantity to item 37, for the unpolarized power spectrum. The unpolarized power was obtained in a manner similar to that used to compute polarized power. Letting

Appendix VI (cont.)

$P_u(k)$  represent the unpolarized power spectra, and referring to the figure below, the unpolarized power is given by

$$U = \sum_{\tilde{B}_1}^{\tilde{B}_2} (P_u(k) - \tilde{n}),$$

where the tildas refer to the values of B and n used in the unpolarized power spectrum. In general, the limits for the polarized and unpolarized echoes were different, as was the value of the system noise level. The difference in frequency limits arose from the difference in the spectral distribution of the unpolarized power; the difference in system noise temperature arose from the signal processing used to separate these quantities (cf Subtask 4, 5). The value of  $\tilde{n}$  was chosen in a manner similar to that of n in item 37. In some cases, it was not clear that all the unpolarized power is contained in the receiver passband. In this event,  $\tilde{B}_1$  or  $\tilde{B}_2$  was set equal to the upper or lower frequency limit as appropriate.



40. Normalized Unpolarized Power is the analogous quantity to item 38, for the unpolarized power spectrum. The normalized unpolarized power is defined as

$$\text{normalized unpolarized power} = U/\tilde{n}$$

where the symbols have the same meaning as in item 39. Comments given under item 38 are also germane to normalized unpolarized power.

- \*  
41. Equivalent Area Bandwidth: the spectrum of a bistatic-radar echo from a well behaved surface may be written as (Fjeldbo, 1964):

$$S(f) = e^{-\frac{\pi^2 f^2}{2}} \left[ 4v_s (\pi/\lambda) \cos \phi \left( \frac{h_o}{d_o} \right) \right]^{-2} = e^{-f^2/2\tilde{\sigma}^2},$$

where

$f$  = frequency measured from the centroid of the echo spectrum

$v_s$  = speed of the specular point across the mean lunar surface

$\lambda$  = wavelength

$\phi$  = angle of incidence, and

$h_o/d_o$  = unidirectional rms slope.

---

\*The three machine calculated bandwidths, i.e., the equivalent area bandwidth, the absolute moment bandwidth, and the second moment bandwidth, provide three quasi-independent methods of determining the spectral width of the received echoes. The equivalent area bandwidth provides a standard result that is not particularly sensitive to the gaussian, or non-gaussian nature of the echo spectrum. The absolute moment bandwidth and the second moment bandwidth so emphasize departures from gaussian because of the increasing importance given to the wings of the spectrum.

Equivalent area bandwidths have been used to determine lunar rms slopes. The absolute moment bandwidths and the second moment bandwidths, when normalized by the equivalent area bandwidth, give a sensitive measure of the departures of the echo spectra from the gaussian conditions. RMS slopes derived from these measures are termed "gaussian equivalent slopes" in that they would correspond to true surface conditions for a surface with gaussian statistics and a gaussian autocorrelation function with the same equivalent widths. A more complete description of the lunar slopes requires additional analysis (e.g., see Parker and Tyler, 1973).

Appendix VI (cont.)

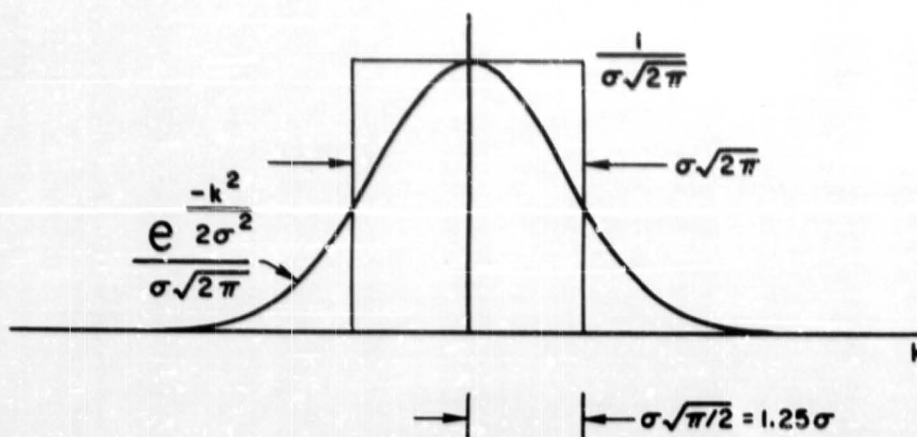
Solving for rms slope in terms of measured values of standard deviation,  $\hat{\sigma}$ , of an experimental spectrum yields

$$h_o/d_o = \frac{\hat{\sigma}}{2(v_s/\lambda) \cos \phi} .$$

Thus, the rms slope may be readily determined from an experimental curve in terms of the  $e^{-1}$  width of that curve. The equivalent area bandwidth is a measure of  $\hat{\sigma}$  based on an equivalent rectangular spectrum of the same area as the experimental spectrum. This width is computed as

$$\hat{\sigma}_{ea} = \frac{\sum_{C_1}^{C_2} P_p(k)}{\max P_p(k)} \cdot (2\pi)^{-1/2}, \quad C_1 < k < C_2.$$

Referring to the figure which follows, the quantity  $\hat{\sigma}_{ea} = \sigma$  if the observed curve is gaussian and noiseless. For non-gaussian data  $\hat{\sigma}_{ea}$  is still a measure of the bandwidth, although the interpretation must be modified. RMS slopes determined from  $\hat{\sigma}_{ea}$  and the expression immediately above will be referred to as equivalent area slopes. The quantity  $\hat{\sigma}_{ea}$  is the equivalent area bandwidth.



42. Normalized Absolute Moment Bandwidths are based on an equivalent value of  $\hat{\sigma}$  computed from the absolute moment of the data. That is,

$$\hat{\sigma}_{am} = \frac{\sum_{k=C_1}^{C_2} P_p(k) |k - \bar{k}|}{\sum_{k=C_1}^{C_2} P_p(k)} \cdot \sqrt{\frac{\pi}{2}}; \quad \bar{k} = \frac{\sum_{k=C_1}^{C_2} P_p(k) k}{\sum_{k=C_1}^{C_2} P_p(k)}$$

for a gaussian spectrum the equivalent area moments and the absolute moments will be equal

$$\hat{\sigma}_{am} = \hat{\sigma}_{ea} = \sigma$$

where the symbols have the same meaning as in item 41.

The normalized absolute moment bandwidth is

$$\hat{\sigma}_{am} / \hat{\sigma}_{ea}$$

For a gaussian echo spectrum this ratio will be unity.

43. Normalized Second Moment Bandwidth: the second moment bandwidth is also based on gaussian equivalence. This bandwidth is defined as

$$\hat{\sigma}_{sm}^2 = \frac{\sum_{k=C_1}^{C_2} P_p(k) (k-\bar{k})^2}{\sum_{k=C_1}^{C_2} P_p(k)}; \quad \bar{k} = \frac{\sum_{k=C_1}^{C_2} P_p(k) \cdot k}{\sum_{k=C_1}^{C_2} P_p(k)} .$$

For a gaussian echo spectrum

$$\hat{\sigma}_{sm} = \hat{\sigma}_{am} = \hat{\sigma}_{ea} = \sigma,$$

where the symbols have the same meaning as under items 42 and 41.

The normalized second moment bandwidth is given by

$$\hat{\sigma}_{sm} / \hat{\sigma}_{ea}.$$

Again, departures of this ratio from unity are indicative of a non-gaussian received echo spectrum

44. Centroid of the Echo Spectrum: the centroid of the echo spectrum is defined in the standard way:

$$\bar{k} = \frac{\sum_{k=C_1}^{C_2} P_p(k) \cdot k}{\sum_{k=C_1}^{C_2} P_p(k)}$$

where the symbols have the same meaning as in 41, 42 and 43. The values of  $C_1$ ,  $C_2$  are held constant throughout items 41, 42, 43 and 44. The echo spectrum centroid is used in the computations of the absolute moment bandwidths and the second moment bandwidths. It is also useful for estimation of the observed doppler difference (cf item 31). However, the centroid has no direct meaning in an

Appendix VI (cont.)

absolute sense because the transmitter frequencies from the spacecraft are not known precisely.

45. RMS Slopes are obtained from the equivalent area bandwidths according to

$$\frac{h_o}{d_o} = \frac{\hat{\sigma}_{ea}}{2(v_s/\lambda) \cos \phi}$$

and

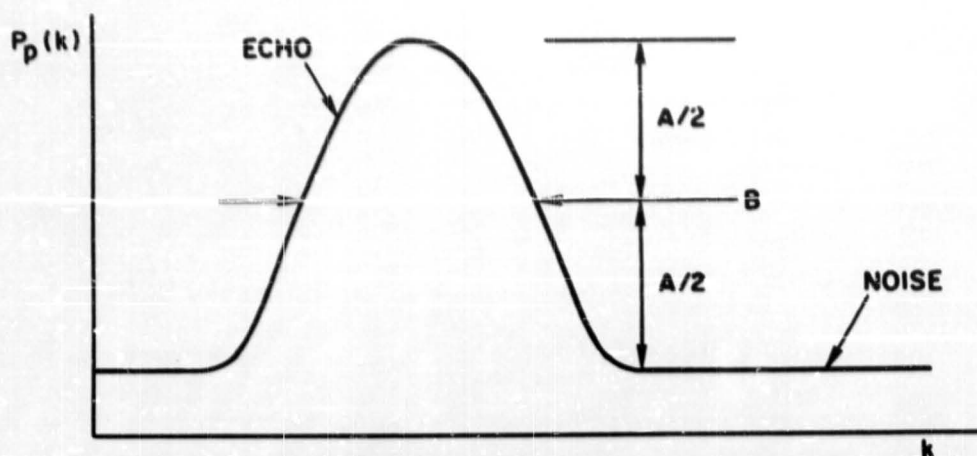
$$\text{unidirectional rms slope (deg.)} = \tan^{-1} (h_o/d_o),$$

where the results are expressed in degrees for convenience. The quantities  $v_s$ ,  $\lambda$ ,  $\phi$  and  $\hat{\sigma}_{ea}$  have been defined in item 41.

46. Handscaled 1/2 Power Echo Bandwidths: handscaling of polarized echo bandwidths has been discussed previously under Subtask 10. A 1/2 power echo bandwidth is defined as the quantity "B" in the figure which follows. In practice, this value was obtained by handscaling data from plots. The handscaled bandwidths provide a rapid, simple technique for the evaluation of lunar rms surface slopes. The handscaled bandwidths were also used as a controlling parameter in development of automated techniques for obtaining echo bandwidths. RMS slopes may be obtained from the handscaled bandwidths by

$$\text{rms slope} = 5.7^{\circ} \times \frac{B}{(\text{predicted 1/2 power bandwidth for rms slope of 0.1})},$$

where the result is given in degrees for convenience. Predicted 1/2 power bandwidths for 0.1 rms slopes are given in word no. 30 of the integral tape data records. Hand measurements were made only for selected segments of the data.



47. Flag: the flag word contains a seven level binary code that indicates data quality. A bit in the "1" condition indicates the existence of a special condition in the data. A bit position in the "0" state carries no meaning other than that the data are normal.

The interpretation of the bit positions is as given below.

<u>Bit in "1" Condition</u>	<u>Implication</u>
1	Polarized power data questionable or no good
2	Unpolarized power data questionable or no good
3	Polarized noise level, $n$ , (cf item 37) changed this data record
4	Polarized integration bounds $B_1, B_2$ , (cf item 37) changed this data record
5	Unpolarized noise level, $\tilde{n}$ , (cf item 39) changed this data record
6	Unpolarized integration bounds, $\tilde{B}_1, \tilde{B}_2$ , (cf item 39) changed this data record
7	System gain changed this data record

## Appendix VI (cont.)

### Explanation

#### Bit Position "1"

Polarized data may be flagged for any one of a number of reasons. The presence of interference, an error in setting the integration bounds, or a tape drive error in the data processing are examples of difficulties that would result in such a flag. In case of gross errors the flag represents an objectively known bad data point. In the case of a more subtle phenomenon such as interference, the flag represents an experimenter's subjective opinion. For the 116 cm data interference is the predominant cause of a data bad flags. Data users who wish to examine this question for themselves may do so by reprocessing the data from the JM Doptrack tapes. It is very strongly recommended that no flagged data be used without taking this precaution.

#### Bit Position "2"

Unpolarized data may be flagged for the same reasons as those given for the polarized data under bit position "1" above. However, because gross errors for polarized and unpolarized data may be independent, and because the unpolarized data possess a certain immunity to interference, which tends to be polarized, the flags in bit position "1" and "2" are not necessarily coincident. As before, in the case of interference, the investigator's judgment is involved.

#### Bit Position "3"

This flag is set when the noise level, i.e.,  $n$  in item 37, is changed during the data reduction process. This flag serves to alert the user that such a change has been made. Any discontinuity that occurs when this bit is set is likely to result from this cause. In the case of the polarized power such discontinuities are generally quite small, on the order of 1%. However, in the case of the normalized polarized power such discontinuities may be large, on the order of two. Obviously, no physical significance should be attached to such discontinuities.

Appendix VI (cont.)

Bit Position "4"

Changes in the integration bounds are flagged for reasons similar to those given under bit position "3". The bounds,  $B_1$ ,  $B_2$ , vary with the changing width and location of the polarized echo. Usually, such changes are very small and their effect is not noticeable in the data.

Bit Position "5"

Changes in the unpolarized noise level,  $\tilde{n}$ , are made for the same reasons as those described under bit position "3". As before, changes in the unpolarized power, and especially the normalized unpolarized power, that occur with these changes in  $\tilde{n}$  are non-physical.

Bit Position "6"

The comments that apply to the polarized integration bounds given under bit position "4" also apply here.

Bit Position "7"

System gain changes may occur during data reception in the receiving systems or during data playback in the record reproduction system. Such changes are flagged since they will appear as a change in the polarized and unpolarized signal levels. Gain changes do not affect measures of echo bandwidths.

48. Antenna Gain is the gain of the spacecraft antenna in the  $\alpha_s$ ,  $\beta_s$  direction determined from antenna patterns contained in NAA (1966b) (116 cm), MSC (1967) (Apollo 14, 13 cm), or NAA (1969) (Apollos 15 and 16, 13 cm).

49. Not Used

50. Sequence Number, where the first data record=1.

Appendix VII

Cross-Reference Table for JM Doptrack/Integral Tape Trajectory Parameters

The table below provides a cross-reference between the JM Doptrack trajectory parameter records and the Integral tape data records. JM Doptrack tapes are described in Appendix IV. That appendix gives the detailed format for those tapes, but does not define all of the trajectory parameters. Integral tapes are described in detail in Appendix VI. That appendix does include a detailed description of the various trajectory parameters. All of the trajectory parameters given on the JM Doptrack tapes are also found on the Integral tapes. This appendix provides a convenient means for determining the location of a given JM Doptrack tape trajectory parameter in the Integral tape format. For reference, the trajectory parameters are found in the sixth record of a data frame on the JM Doptrack tape (i.e., in record number  $N \cdot 6$ ,  $N = 1, 2, 3, \dots$ , where the first data record = 1).

<u>JM Doptrack</u> <u>Word No.</u>	is found in	<u>Integral Tape</u> <u>Word No.</u>
1		1
2		2
3		31
4		30
5		28
6		34
7		9
8		35
9		36
10		3
11		4
12		5
13		13
14		14
15		15
16		24
17		25
18		33

Appendix VII (cont.)

<u>JM Doptrack</u>		<u>Integral Tape</u>
<u>Word No.</u>	is found in	<u>Word No.</u>
19		32
20		26
21		27
22		29
23		22
24		23
25		16
26		17
27		18
28		6
29		7
30		8
31		10
32		11
33		12

Units and scale factors are identical on JM Doptrack and Integral tapes.

Appendix VIII

Matrix Correction Factors

The tables below give the matrix correction factors (c-matrix) that were applied to the 116 cm data in Subtask 5 (cf text). No corrections were applied to the 13 cm data.

In all cases, the following values were used for  $C_{12}$  and  $C_{22}$

$$C_{12} = 0.0 + j 0.0$$

$$C_{22} = 1.0 + j 0.0$$

Only  $C_{11}$  and  $C_{21}$  were varied. Start times shown below refer to the time on the first frame to which the particular c-matrix was applied; the same c-matrix was used on all succeeding frames with times less than the next entry in the table.

Apollo 14

Time UT2 (sec) start	C-matrix	
	$C_{11}$	$C_{21}$
23338.35	1.100 + j 0.0	0.0 + j 0.0
25155.63	1.960 + j 0.0	0.050 + j 0.200
25166.28	1.230 + j 0.0	0.070 + j 0.150
25168.94	1.100 + j 0.0	0.0 + j 0.0
25190.24	1.200 + j 0.0	0.0 + j 0.07
25192.91	1.960 + j 0.0	0.050 + j 0.200
25198.23	1.200 + j 0.0	0.0 + j 0.070
25206.22	1.100 + j 0.0	0.0 + j 0.0
26348.41	0.929 + j 0.0	0.189 + j 0.0

Apollo 15

all data	C-matrix	
	$C_{11}$	$C_{21}$
	1.000 + j 0.0	0.0 + j 0.0

Appendix VIII (cont.)

Apollo 16

Time UT2 (sec)	C-matrix	
start	$c_{11}$	$c_{21}$
4592.35	$0.913 + j 0.0$	$-0.134 - j 0.045$
4780.77	$0.958 + j 0.0$	$-0.040 - j 0.010$
5432.35 <sup>α</sup>	$0.944 + j 0.0$	$-0.055 - j 0.032$
5587.79	$1.000 + j 0.0$	$-0.060 + j 0.020$
5983.46	$0.900 + j 0.0$	$-0.100 - j 0.050$
6272.35 <sup>α</sup>	$0.830 + j 0.0$	$-0.100 - j 0.040$
6484.32	$0.870 + j 0.0$	$-0.090 + j 0.0$
7030.72	$0.860 + j 0.0$	$-0.060 - j 0.050$
7112.35 <sup>α</sup>	$0.871 + j 0.0$	$-0.072 - j 0.490$
7333.74	$0.815 + j 0.0$	$-0.066 + j 0.010$
7701.15	$0.778 + j 0.0$	$-0.060 - j 0.040$
7952.35 <sup>α</sup>	$0.740 + j 0.0$	$-0.100 - j 0.040$

<sup>α</sup>These changes are located in overlap areas described in Appendix IV (D3).  
 The change takes effect on the frame with the time (word 2, record 6;  
 cf Appendix IV) closest to that shown here.

## Appendix IX

### Coordinate Transformations

#### A. General Definitions

$\bar{r}$  = specular point position vector

$\bar{p}$  = spacecraft position vector

$\bar{v}$  = spacecraft velocity vector

$\bar{a}_{\Delta H}$  = vector in local horizon system

$\bar{a}_{\Delta V}$  = vector in vehicle reference frame

$\bar{a}_{\Delta P}$  = vector in primary or principal reference system

$\left. \begin{array}{l} \emptyset \\ \Psi \\ \theta \end{array} \right\}$  defined in C below (Euler angles between local horizon and vehicle systems)

$\left. \begin{array}{l} \alpha \\ \beta \end{array} \right\}$  look angles to specular point in vehicle system

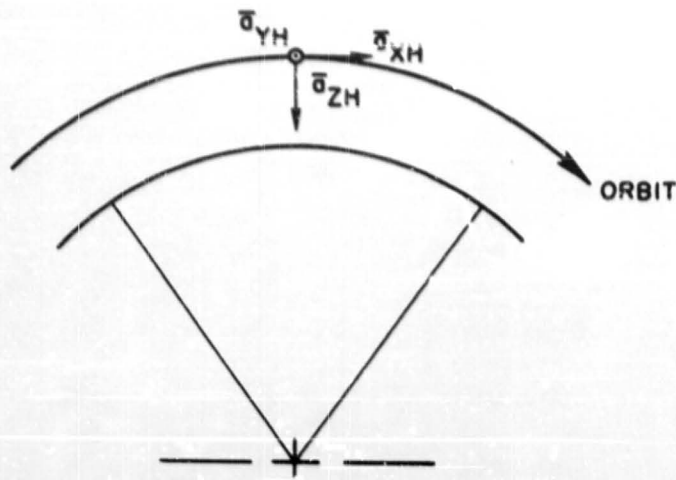
$\delta$  } orientation of vehicle along  $\alpha, \beta$  direction (defined below)

B. Data supplied by MSC gives spacecraft attitude in "Local Horizontal" coordinate system.

Definition of "Local Horizontal" system (see figure which follows):

$$\begin{aligned}\bar{a}_{ZH} &= - \frac{\bar{p}}{|\bar{p}|} \\ \bar{a}_{YH} &= \frac{\bar{v} \times \bar{p}}{|\bar{v} \times \bar{p}|} \\ \bar{a}_{XH} &= \bar{a}_{YH} \times \bar{a}_{ZH}.\end{aligned}$$

Appendix IX (cont.)



$\bar{a}_{ZH}$  is directed toward the nadir.

$\bar{a}_{YH}$  is directed along angular momentum vector.

$\bar{a}_{XH}$  is in the plane of the orbit roughly along  $\bar{v}$ .

C. Specification of spacecraft attitude

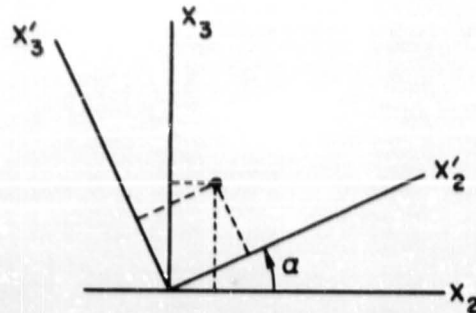
The Euler angles  $\emptyset, \Psi, \theta$  specify the sequence of rotations required to transform Local Horizontal coordinates to Vehicle coordinates as follows:

$$\begin{bmatrix} X_V \\ Y_V \\ Z_V \end{bmatrix} = \begin{bmatrix} \emptyset \\ (X) \end{bmatrix} \begin{bmatrix} \Psi \\ (Z) \end{bmatrix} \begin{bmatrix} \theta \\ (Y) \end{bmatrix} \begin{bmatrix} X_H \\ Y_H \\ Z_H \end{bmatrix}$$

where the matrix  $\begin{bmatrix} \text{(ang)} \\ \text{(axis)} \end{bmatrix}$  denotes a rotation of (ang) about the current (axis). Rotations are in the sequence (Y, Z, X). The sense of rotation is clockwise when looking in the + (axis) direction. For instance, consider:

Appendix IX (cont.)

$$\begin{bmatrix} x'_1 \\ x'_2 \\ x'_3 \end{bmatrix} = \begin{bmatrix} \alpha \\ (x_1) \end{bmatrix} \begin{bmatrix} x_1 \\ x_2 \\ x_3 \end{bmatrix}$$



$$x'_1 = x_1$$

$$x'_2 = x_2 \cos\alpha + x_3 \sin\alpha$$

$$x'_3 = -x_2 \sin\alpha + x_3 \cos\alpha$$

then the transformation is

$$\begin{bmatrix} x'_1 \\ x'_2 \\ x'_3 \end{bmatrix} = \begin{bmatrix} 1 & 0 & 0 \\ 0 & \cos\alpha & \sin\alpha \\ 0 & -\sin\alpha & \cos\alpha \end{bmatrix} \begin{bmatrix} x_1 \\ x_2 \\ x_3 \end{bmatrix}$$

Thus

$$\begin{bmatrix} \emptyset \\ (X) \end{bmatrix} \begin{bmatrix} \Psi \\ (Z) \end{bmatrix} \begin{bmatrix} \theta \\ (Y) \end{bmatrix} = \begin{bmatrix} R \end{bmatrix}$$

$$\begin{bmatrix} R \end{bmatrix} = \begin{bmatrix} \cos\Psi \cos\theta & \sin\Psi & -\cos\Psi \sin\theta \\ \sin\emptyset \sin\theta - \cos\emptyset \sin\Psi \cos\theta & \cos\emptyset \cos\Psi & \cos\emptyset \sin\Psi \sin\theta + \sin\emptyset \cos\theta \\ \sin\emptyset \sin\Psi \cos\theta + \cos\emptyset \sin\theta & -\sin\emptyset \cos\Psi & \cos\emptyset \cos\theta - \sin\emptyset \sin\Psi \sin\theta \end{bmatrix}$$

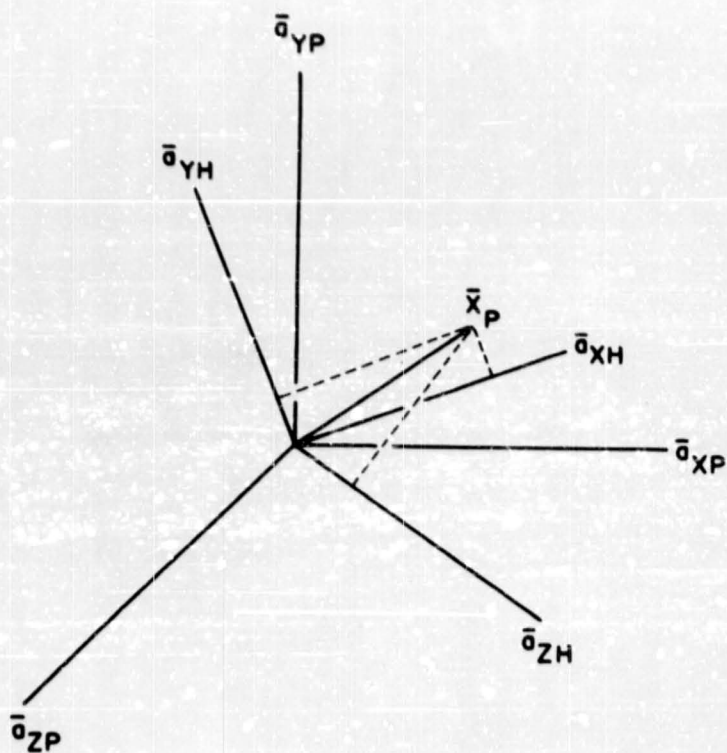
D. Conversion of Reference Coordinate to Local Horizontal System

Quantities that are known in the principal reference system may be converted to the Local Horizon system through the directional cosines connecting the two. These are given by the vector components of the  $\bar{a}_{\Delta H}$ , expressed in the primary system. The  $\bar{a}_{\Delta H}$  form the rows of the

Appendix IX (cont.)

transformation (rotation only) matrix. Thus

$$\begin{bmatrix} \bar{x}_H \\ \bar{y}_H \\ \bar{z}_H \end{bmatrix} = \begin{bmatrix} a_{XH_1} & a_{XH_2} & a_{XH_3} \\ a_{YH_1} & a_{YH_2} & a_{YH_3} \\ a_{ZH_1} & a_{ZH_2} & a_{ZH_3} \end{bmatrix} \begin{bmatrix} \bar{x}_P \\ \bar{y}_P \\ \bar{z}_P \end{bmatrix}$$



Components in sub -H system are projections onto reference axes of that system.

Appendix IX (cont.)

E. Conversion of Reference Coordinates for Vehicle Coordinates

Conversion from principal coordinates to Vehicle coordinates may be made by two successive rotations, principal coordinates  $\rightarrow$  Local Horizontal coordinates Local Horizontal coordinates  $\rightarrow$  Vehicle coordinates.

or

$$\begin{bmatrix} \bar{x}_V \end{bmatrix} = \begin{bmatrix} R_{VH} \end{bmatrix} \begin{bmatrix} x_H \end{bmatrix} = \begin{bmatrix} R_{VH} \end{bmatrix} \begin{bmatrix} R_{HP} \end{bmatrix} \begin{bmatrix} \bar{x}_P \end{bmatrix}$$

where  $R_{ij}$  implies a rotation from the  $j$  to  $i$  system. Thus  $\begin{bmatrix} R_{VP} \end{bmatrix} = \begin{bmatrix} R_{VH} \end{bmatrix} \begin{bmatrix} R_{HP} \end{bmatrix}$ .

F. Computation of spacecraft to specular point look angles,  $\alpha_s, \beta_s$ .

1. The direction to the specular point from the spacecraft is

$$\frac{\bar{r} - \bar{p}}{|\bar{r} - \bar{p}|} = \bar{\gamma}.$$

In Vehicle coordinates

$$\bar{\gamma}_V = \begin{bmatrix} R_{VP} \end{bmatrix} \begin{bmatrix} \bar{\gamma}_P \end{bmatrix}.$$

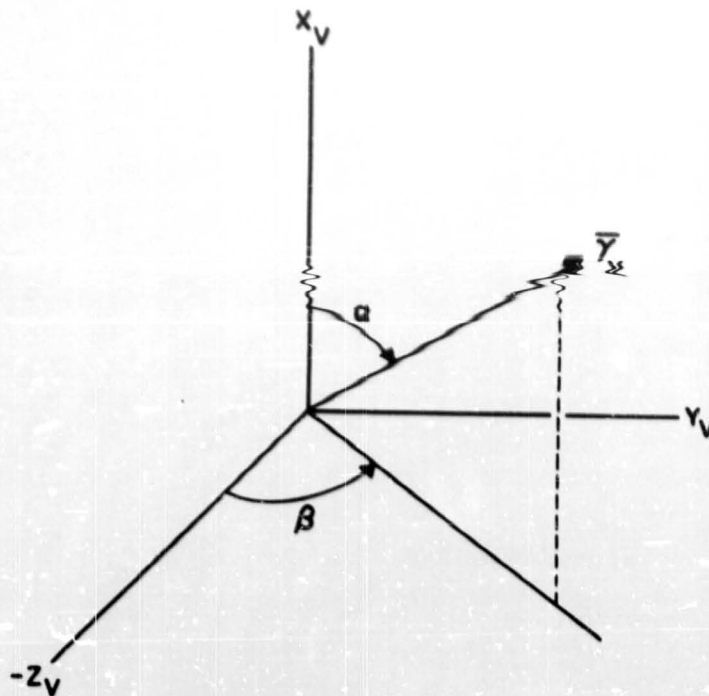
The quantity  $\alpha$  is measured from the + X direction,

$$\therefore \alpha_s = \arccos(\gamma_{XV}), \quad 0 \leq \alpha \leq \pi.$$

The quantity  $\beta_s$  is the azimuthal angle (minimum angle to  $\bar{\gamma}$ ,  $X_V$  plane) measured from the  $-Z_V$  axis, positive towards  $+Y_V$ :

$$\beta_s = \text{signum}(\gamma_{YV}) \cdot \arccos(-\gamma_{ZV}), \quad -\pi \leq \beta \leq \pi,$$

where  $\text{signum}(X) = \frac{X}{|X|}$ . These quantities are depicted in the figure which follows:



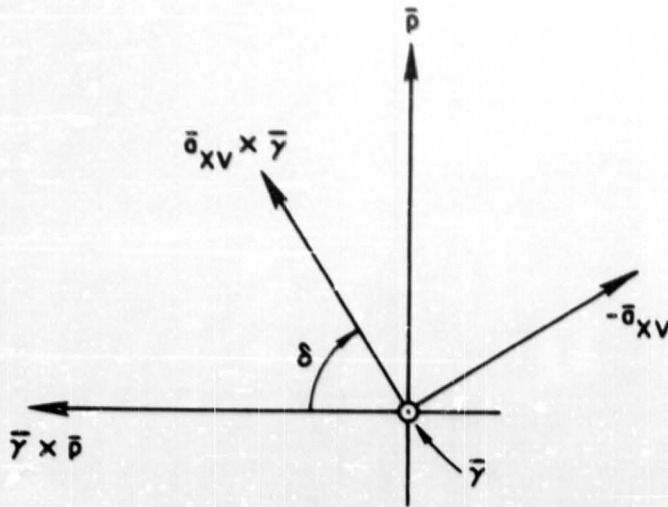
G. Definition and Computation of  $\delta$ .

The angle  $\delta$  is the included angle between the  $\bar{\gamma}, \bar{a}_{XV}$  plane and the plane of incidence, the  $\bar{\gamma}, \bar{p}$  plane (see figure which follows):

$$\delta = \text{signum}(\bar{p} \cdot \bar{a}_{XV} \otimes \bar{\gamma}) \cdot \arccos \left( \frac{\bar{\gamma} \otimes \bar{p}}{\bar{\gamma} \otimes \bar{p}} \cdot \frac{\bar{a}_{XV} \otimes \bar{\gamma}}{\bar{a}_{XV} \otimes \bar{\gamma}} \right),$$

$$-\pi \leq \delta \leq \pi.$$

Appendix IX (cont.)



H. Sources

Additional information regarding the definitions of Local Horizon and Vehicle coordinates may be found in MSC publications describing trajectory tapes (MSC, 1970). Input for  $\alpha_s$ ,  $\beta_s$ ,  $\delta$  computations are MSC supplied experimenter trajectory tapes. The principle reference frame is selenographic.

## Appendix X

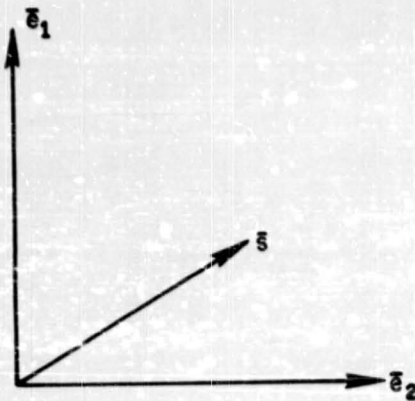
### Relationship Between the Coherency Matrix and Other Specifications of Polarization

The methods used to estimate the polarization state of Apollo bistatic-radar data are those described by Tyler and Simpson, (1970). This appendix describes the relationship of the coherency matrix to the more common descriptors intensity, axial ratio and orientation of the polarization ellipse.

The coherency matrix is from Born and Wolf, (1959).

$$\bar{e}_1(t) = \text{Re} \left\{ E_1 e^{j\omega t} \right\} \bar{e}_1$$

$$\bar{e}_2(t) = \text{Re} \left\{ E_2 e^{j\omega t} \right\} \bar{e}_2$$



$$\underline{J} = \begin{bmatrix} \langle E_1 E_1^* \rangle & \langle E_1 E_2^* \rangle \\ \langle E_1^* E_2 \rangle & \langle E_2 E_2^* \rangle \end{bmatrix}$$

where  $E_1, E_2$  are complex magnitudes associated with any pair of orthogonal linear polarizations.

$$\underline{J} = \begin{bmatrix} J_{11} & J_{12} \\ J_{21} & J_{22} \end{bmatrix}; \quad J_{ij} = \langle E_i E_j^* \rangle$$

Appendix X (cont.)

$$\underline{\rho} = \text{Tr}(\underline{J}) \begin{bmatrix} \rho_{11} & \rho_{12} \\ \rho_{21} & \rho_{22} \end{bmatrix}; \text{Tr}(\underline{J}) = J_{11} + J_{22} = \text{total received power}$$

Born and Wolf show that the percentage polarization  $\gamma$ , i.e., the fraction of  $\text{Tr}(\underline{J})$  that may be described by a deterministic polarization ellipse, is

$$\gamma = \sqrt{1 - 4(\rho_{11}\rho_{22} - \rho_{12}\rho_{21})}$$

Then any  $\underline{J}$  may be written as

$$\underline{J} = \underbrace{\frac{1}{2}(1 - \gamma) \text{Tr}(\underline{J}) \begin{bmatrix} 1 & 0 \\ 0 & 1 \end{bmatrix}}_{\text{unpolarized part}} + \underbrace{\gamma \text{Tr}(\underline{J}) \begin{bmatrix} q_{11} & q_{12} \\ q_{21} & q_{22} \end{bmatrix}}_{\text{polarized part}}$$

where

$$q_{ii} = \frac{1}{\gamma} (\rho_{ii} - \frac{1}{2}(1-\gamma)); \quad q_{ij} = \frac{1}{\gamma} \rho_{ij}$$

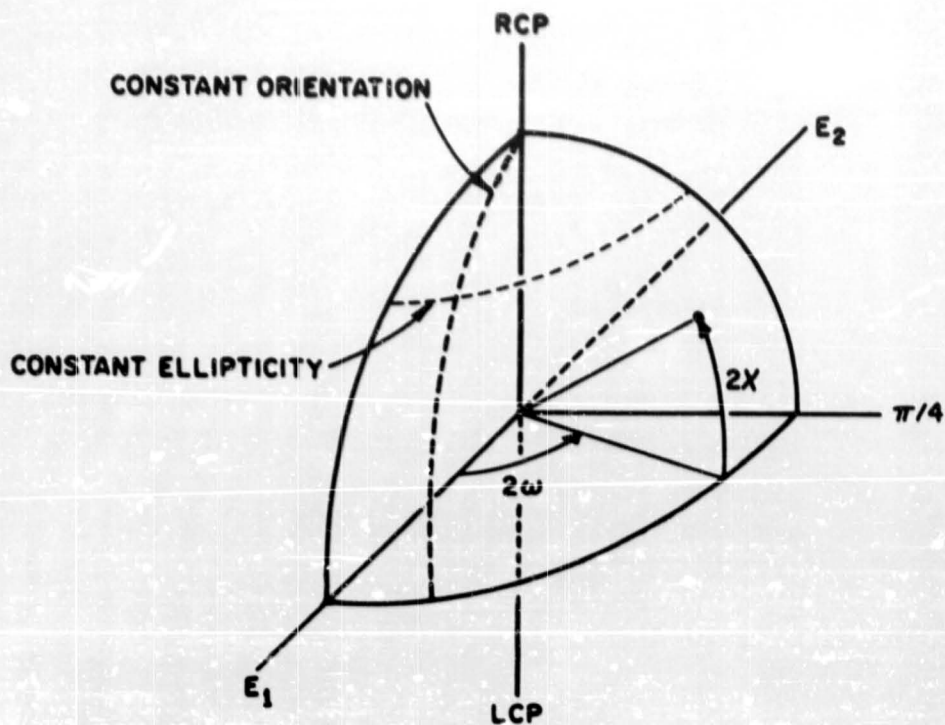
Ko (1962) gives the relationship between  $\underline{q}$  and the Poincaré sphere (Beckmann, 1968) as: (shown schematically in the figure which follows)

$$q_{11} = \cos 2\omega, \quad 0 \leq \omega \leq \pi$$

$$q_{12} = \sin \omega \cos \omega e^{j2\chi} \Rightarrow \tan 2\chi = \frac{\text{Im}(q_{12})}{\text{Re}(q_{12})}, \quad -\frac{\pi}{2} < 2\chi < \frac{\pi}{2}$$

Also note:

$$\tan \omega = \sqrt{\frac{q_{22}}{q_{11}}}, \quad \tan \chi = \frac{M}{N}, \quad \tan \chi > 0 \Rightarrow \text{right elliptical polarization.}$$



For Apollo, a similar matrix  $\underline{J}_c$ , where the sub-c designates decomposition of the incident wave into circular components, is used:

$$\underline{J}_c = \begin{bmatrix} \langle E_l E_l^* \rangle & \langle E_l E_r^* \rangle \\ \langle E_l^* E_r \rangle & \langle E_r E_r^* \rangle \end{bmatrix} \quad \begin{bmatrix} J_{c11} & J_{c12} \\ J_{c21} & J_{c22} \end{bmatrix} \quad \text{where } E_l \text{ and } E_r \text{ denote left and right circular waves.}$$

Defining  $\underline{\rho}_c$  and  $\underline{q}_c$  in an analogous manner:

Appendix X (cont.)

$$\underline{J}_c = \begin{bmatrix} \rho_{c11} & \rho_{c12} \\ \rho_{c21} & \rho_{c22} \end{bmatrix} = \frac{1}{2} (1-\gamma) \text{Tr}(\underline{J}_c) \begin{bmatrix} 1 & 0 \\ 0 & 1 \end{bmatrix} + \gamma \text{Tr}(\underline{J}_c) \begin{bmatrix} q_{c11} & q_{c12} \\ q_{c21} & q_{c22} \end{bmatrix}, \text{ where}$$

$$\text{as before } \gamma = \sqrt{1 - 4 (\rho_{c11} \rho_{c22} - \rho_{c12} \rho_{c21})}.$$

However, the interpretation of the  $\underline{q}_c$  is modified in accordance with the new definition:

$$\tan \chi = \frac{M}{N} = \frac{-\sqrt{q_{c11}} + \sqrt{q_{c22}}}{\sqrt{q_{c11}} + \sqrt{q_{c22}}}$$

$$\omega = \frac{1}{2} \arg (q_{12}),$$

where  $\omega$  is referenced to instantaneous  $E_\theta$  position at time  $t = 0$ .

The invariance of  $\text{Tr}(\cdot)$ ,  $\text{Det}(\cdot)$ , and  $\gamma$  under transformations to circular coordinates can be verified by direct computation.

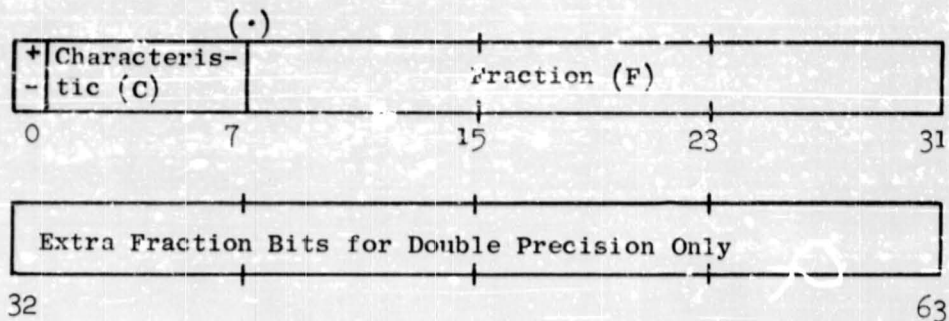
## Appendix XI

### XDS Sigma 5 Machine Images

All data on the JM Doptrack and Integral tapes are in the form of XDS Sigma 5 machine images. One word is 32 bits, one byte, 8 bits. The data are either real (floating-point), integer, or alphanumeric. The machine images are as follows:

#### A. Real

A single precision real number consists of a sign bit (bit 0), a biased<sup>α</sup>, base 16 exponent called a characteristic (bits 1-7), and a 24 bit fraction. A double precision number consists of a single precision number followed by an additional 32 bits of fractional significance (cf figure below). Unless otherwise noted, all numbers referred to in this report as "real" are single precision.



<sup>α</sup>The bias value of  $64_{10}$  is added to the exponent to make it possible to compare the absolute magnitude of two numbers without reference to a sign bit.

Appendix XI (cont.)

A real number (N) is defined as follows:

$$N = F \times 16^{C-64} \text{ where}$$

$$F = 0 \text{ or}$$

$$2^{-24} \leq |F| < 1 \text{ (single precision) or}$$

$$2^{-56} \leq |F| < 1 \text{ (double precision)}$$

$$\text{and } 0 \leq C \leq 127$$

A negative real number is the two's complement of its positive representation. (Note that this differs from the IBM 360.)

B. Integer

Integers are written in full-word, two's complement representation.

C. Alphanumeric

Alphanumeric data, strings of characters, are represented in Extended Binary-Coded-Decimal Interchange Code (EBCDIC). Each character occupies one byte (8 bits), so each word of alphanumeric data contains four characters.

## References

- Beckmann, P., The Depolarization of Electromagnetic Waves, The Golem Press, Boulder, Colorado, 1968.
- Blackman, R. B. and J. W. Tukey, The Measurement of Power Spectra, Dover Publications, Inc., New York, 1958.
- Born, M. and E. Wolf, Principles of Optics, Pergamon Press, New York 1959.
- Howard, H. T. and G. L. Tyler, "Bistatic-Radar Studies of the Lunar Surface," Apollo 14 Preliminary Science Report, NASA publication SP-272, 1971.
- Howard, H. T. and G. L. Tyler, "Bistatic-Radar Investigation," Apollo 15 Preliminary Science Report, NASA publication SP-289, p. 23-1, 1972.
- Howard, H. T. and G. L. Tyler, Apollo 16 Preliminary Science Report, NASA publication SP-315, p. 25-1, November, 1972.
- Ko, H. C., Proc. IRE, pp. 1950-1956, September, 1962.
- Tyler, G. L. and H. T. Howard, "Bistatic-Radar Observations of the Lunar Surface with Apollos 14 and 15," paper presented at Third Lunar Conference, Houston, Texas, January, 1972.
- Tyler, G. L. and D. H. H. Ingalls, "Functional Dependence of Bistatic Radar Frequency Spectra on Lunar Scattering Laws," J. Geophys. Res., Vol. 76, No. 20, pp. 4775-4785, July, 1971.
- Tyler, G. L. and R. A. Simpson, Bistatic-Radar Studies of the Moon with Explorer 35, Final Report: Part 2, Scientific Report No. 3610-2, Stanford Electronics Laboratories, October, 1970.
- Tyler, G. L., Estimation of Polarization with Arbitrary Antennas, Scientific Report No. 3610-1, SU-SEL-70-064, Stanford Electronics Laboratories, October, 1970.
- DSN, 1970, Operations Plan for Apollo 14, Vol. VI, Report No. 609-37, Jet Propulsion Lab., Pasadena, California, 15 December 1970.
- DSN, 1971, Operations Plan for Apollo 15, Vol. VII, Report No. 609-38, Jet Propulsion Lab., Pasadena, California, 1 January 1971.
- DSN, 1972, DSN/Flight Project Interface Design Handbook, Deep Space Network Standard Practice Doc. No. 810-5C, Jet Propulsion Lab., Pasadena, California, 1 April 1972.
- MSC, 1967, Full Scale Block II Command and Service Module S-Band Omni Antenna Patterns, MSC Report No. 67-EE-15, Project Apollo, Manned Spaceflight Center, Houston, Texas, June, 1967.

MSC, 1970, "Apollo Postflight Trajectory Parameters," MSC Internal Note No. 70-FM-21 (MSC-01564), Manned Spaceflight Center, Houston, Texas, 13 February 1970.

MSC, 1970, Bistatic Test Data Package (VHF Spectrum and LM S-Band Interference), "MSC Report No. MSC-EE7-70-115(u), Manned Spaceflight Center, Houston, Texas, 18 December 1970.

NAA, 1966a, Radiation Distribution Plots of Linear Polarization Data Types, Report No. NAA 66H-343, North American Aviation, Columbus, 20 April 1966.

NAA, 1966b, VHF SM/SLA Scimitar Antenna, FDWA M 6547, Second Pattern Report, 2 Vols., Report No. NA 66H-31, North American Aviation, Columbus, 1966 (no further data given).

NAA, 1969, High-Gain Antenna Equipment Characteristics and Operation 106 and Subsequent S/C, Report No. TDR 69-042, Revision 1, North American Rockwell Space Division, Downey, April, 1969.

## NOTES

### Block Diagram I: Block Diagram of Stanford Apollo Bistatic-Radar Data Processing and Reduction

- (1)
  - a) Receiving system described in Appendix I.
  - b) Critical filter response given in Appendix III.
  - c) RCP, LCP, coherency maintained through entire system.
  - d) Antenna pointing maintained toward center of moon using Stanford Research Institute lunar ephemeris.
  - e) Absolute phase in LCP, RCP channels not controlled, relative phase maintained.
  - f) Spectral purity of downlink signals measured for Apollo equipment type (MSC, 1970).
  
- (2)
  - a) Deep space network station under NASA control, used standardized procedures except as noted.
  - b) Apollo operational system used for 64 m dish pointing, closed loop receiver acquisition. Station configuration for bistatic-radar experiment described elsewhere (DSN, 1970, 1971).
  - c) Absolute phase in RCP, LCP not controlled, relative phase maintained.
  
- (3)
  - a) Stanford Signal Conditioning Unit provided critical control over system frequency response. Filter characteristics given in Appendix III.
  - b) FR1400 tape recorders A, B used to provide continuous data across tape changes.
  
- (4)
  - a) H.P. 3955B frequency response adjusted for a maximally flat frequency response on playback using calibration tapes from data source machine (H.P. 3955B for 116 cm data; FR1400 A, B for 13 cm data).
  - b) Coherent sampling maintained. Reference signal from tape used to synchronize samples.
  - c) Actual time recovered by use of time code translator clock output to establish start times. Time from start maintained by counting sampling pulses.

(4) d)	Actual sampling rates: (cont.)		Ratio of Effective Sampling Rate to Actual Sampling Rate	
	Flight	Wavelength	Sampling Rate	
	Apollo 14	13 cm	10.75 kHz	4
	Apollo 14	116 cm	10.00 kHz	1
	Apollo 15	13 cm	10.75 kHz	4
	Apollo 15	116 cm	10.00 kHz	1
	Apollo 16	13 cm	21.5 kHz	2
	Apollo 16	116 cm	10.00 kHz	1

(5) a) Fourier coefficients computed from successive groups of weighted data: data group length either 1024 or 2048 samples, weighting function is  $\sin^2(\pi t/T)^T$ , where t is time and T is duration of sample group length.

b) Data analysis lengths

Data Source	Sample Length	Analysis bandwidth (Hz)
Apollo 14 S-band	1024	42.0
Apollo 14 VHF	1024	9.8
Apollo 15 S-band	1024	42.0
Apollo 15 VHF	2048	4.9
Apollo 16 S-band	1024	42.0
Apollo 16 VHF	2048	4.9

(6) Polarimeter computed elements of signal covariance matrix (see Subtask 5).

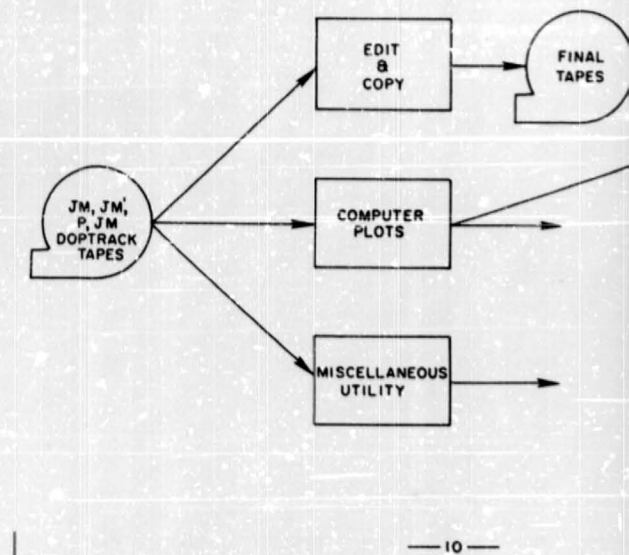
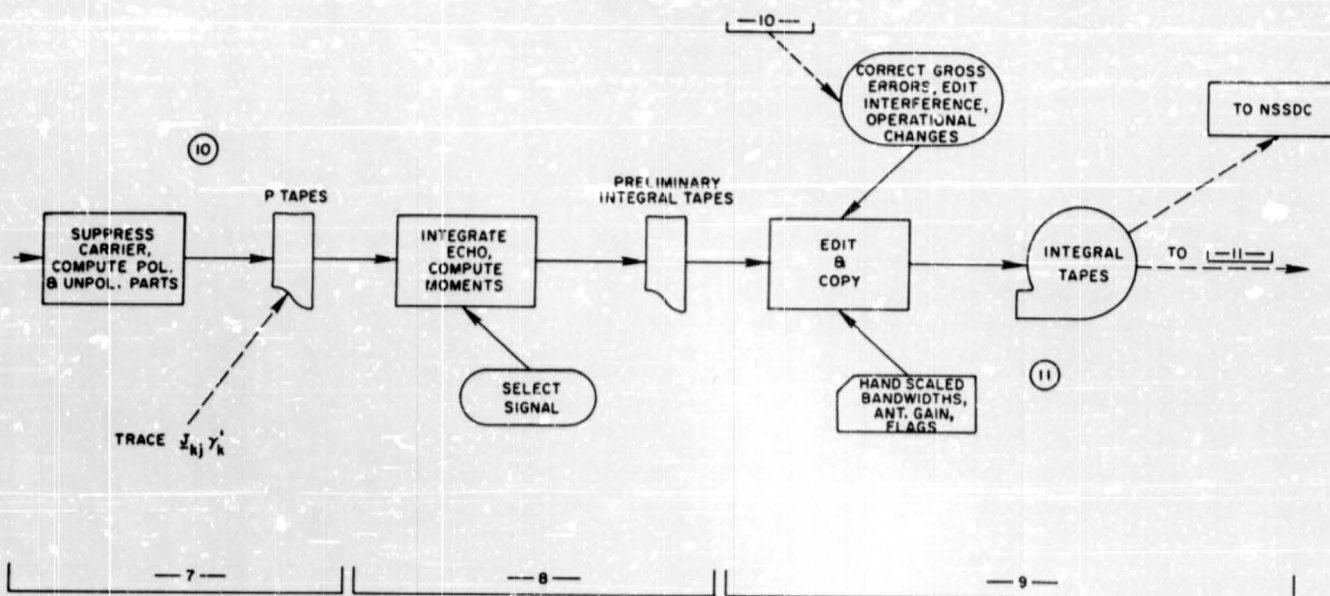
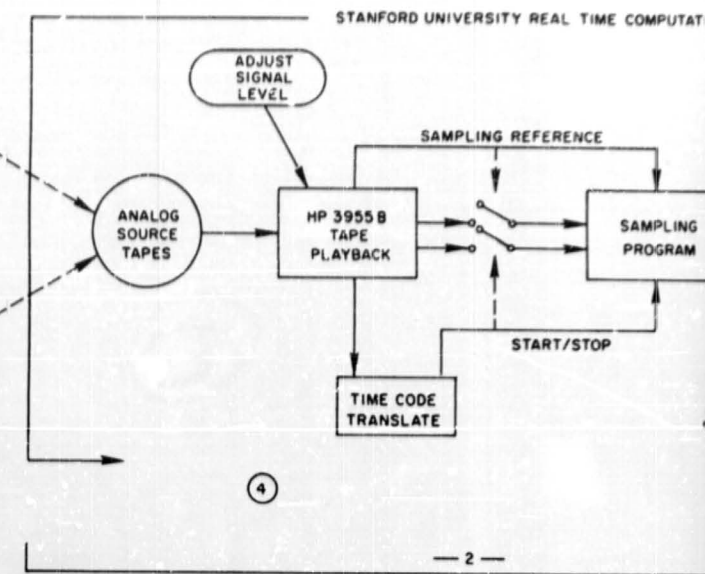
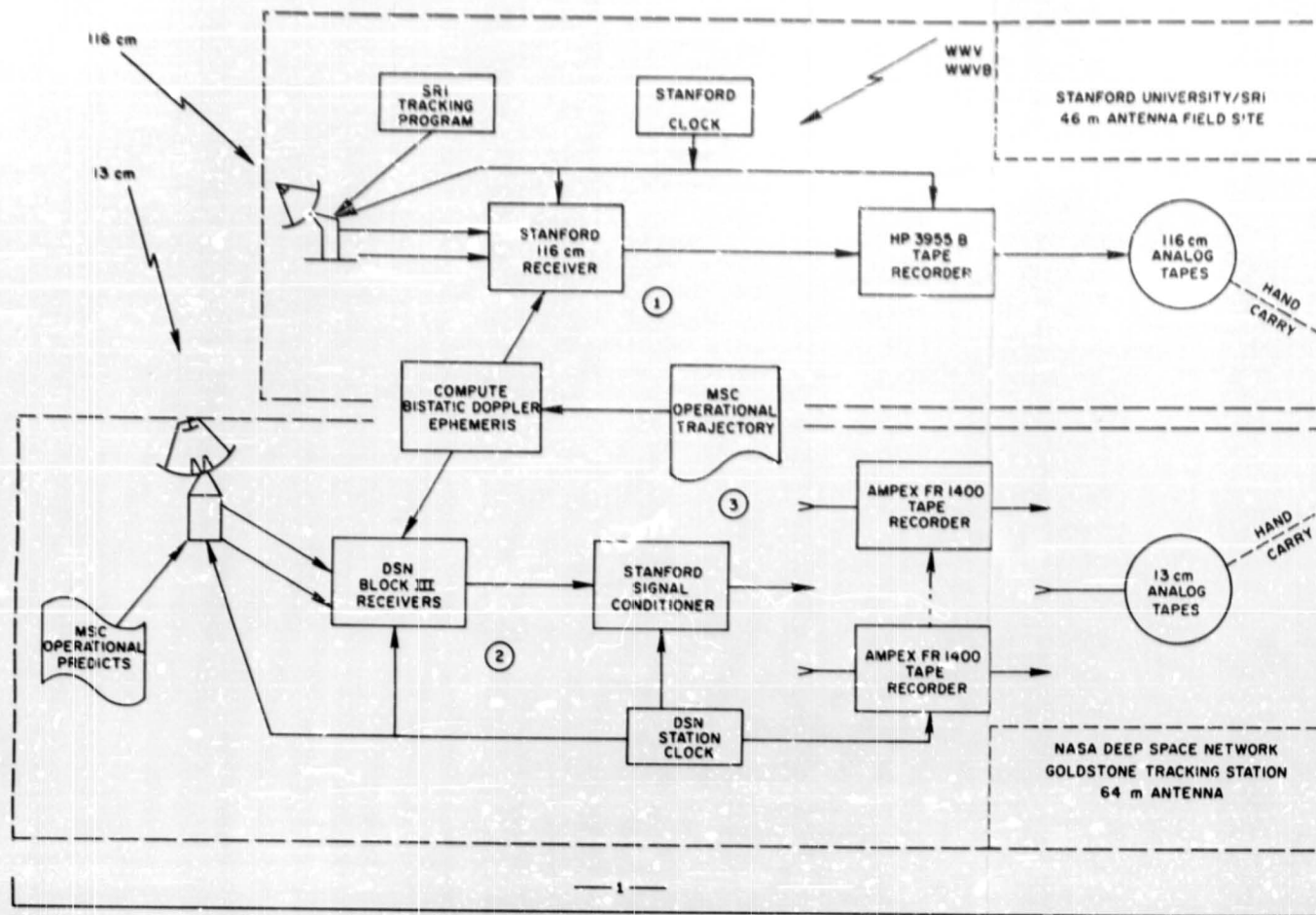
(7) a) Normalizing data obtained from data runs employing noise input. Purpose was to compensate for variations in receiver passband.

b) Normalizing tapes contain smoothed power spectra from noise source data.

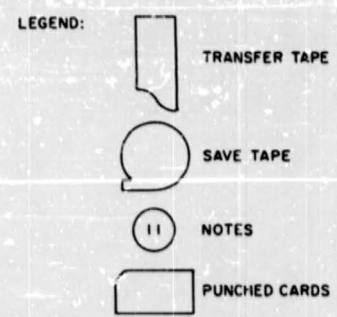
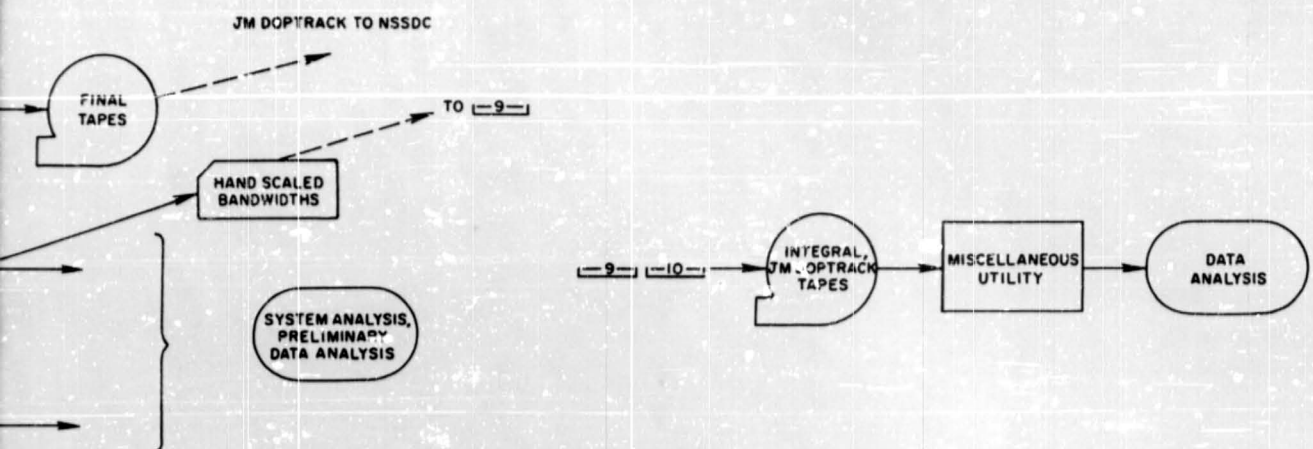
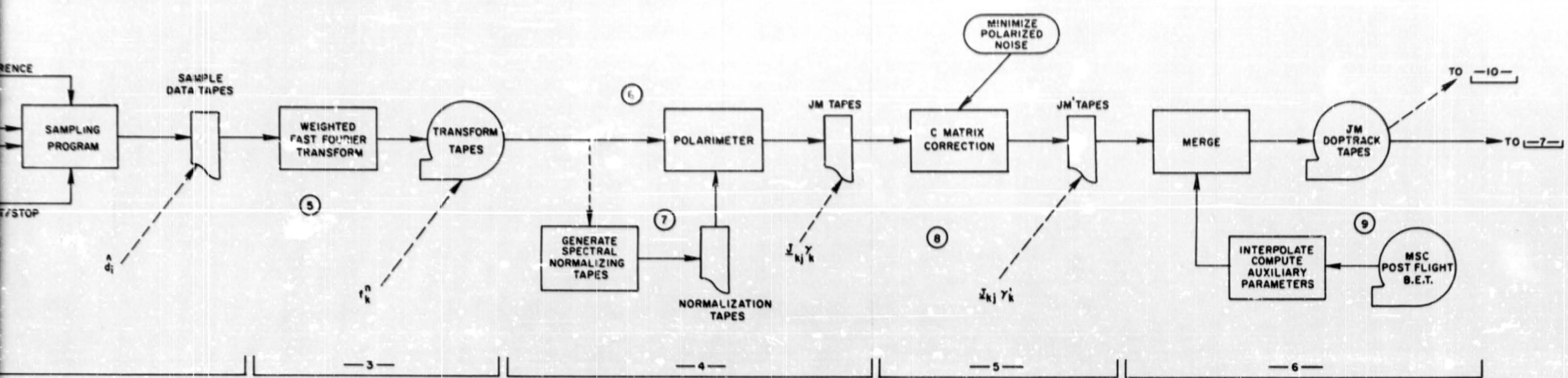
(8) a) C-matrix correction was polarization coordinate transformation to correct for errors in receiver antenna system. Applied to 116 cm data only.

b) Criterion for choosing c-matrix was to minimize polarized part of system noise.

- (9) a) Merge combined data tapes with geometrical parameters obtained from MSC (Best-Estimate-Trajectory) Post-Flight tapes.
- b) MSC data are interpolated to center of data averaging window.
- c) JM Doptrack tapes constitute primary data source for analysis.
- (10) Carrier suppression deleted direct signal from the data by means of an empirical algorithm (see Subtask 7 and Appendix V).
- (11) a) Tapes edited for changes indicated in operational logs and interference.
- b) Handscaled data added to tape from card source.
- c) Edited integral tapes constitute reduced data records.



REAL TIME COMPUTATION FACILITY →



**BLOCK DIAGRAM I:**  
 SIMPLIFIED BLOCK DIAGRAM  
 STANFORD APOLLO BISTATIC-RADAR  
 DATA PROCESSING AND REDUCTION







